NTNU – Trondheim
Norwegian University of
Science and Technology

A method for remote sensing of acoustic ship noise

Stian Coward

Master of Science in Electronics
Submission date: June 2013
Supervisor: Hefeng Dong, IET
Co-supervisor: Dag Tollefsen, Forsvarets forskningsinstitutt

Norwegian University of Science and Technology
Department of Electronics and Telecommunications

Task description

This project shall develop and implement a method for remote measurements of the source level of radiated acoustic noise from marine vessels (ship noise) by use of data from a sensor unit placed on the seabed. The method is of interest as there is increased focus within the EU to monitor and predict ocean noise. Methods to correct the measurements for propagation effects shall be discussed and implemented. The method shall be applied to selected acoustic data from measurements with the NILUS (networked intelligent underwater sensors) measurement platform.

Abstract

Ship noise in the ocean due to commercial shipping has gained increased interest in recent years because of its potential impact on marine life and the ocean environment. Hence, rapid methods to estimate the source level of commercial ships has obtained considerable research interest. Although a number of measurement standards exist that describe measurement procedures for dedicated measurement ranges or well-controlled measurement conditions, there is an interest in methods adapted/developed for non-ideal measurement conditions, such as those of a relatively narrow fjord with considerable shipping activity. This thesis addresses such a non-ideal setting in the context of ship noise measurements with a hydrophone near the seabed in shallow water with ships in passing at long ranges (many times the water depth).

A method for ship-noise source level estimation is formulated that corrects measured (received) levels for background noise, uses a range estimate based on ship Automatic Identification System (AIS) data, and corrects for propagation effects using a complex acoustic propagation model (RAM) with a distributed source model. In addition, the LYBIN propagation model and a simple spherical spreading loss correction is applied alternatively. The goal is monopole ship source levels in 1 Hz bands and 1/3 octave frequency bands. A detailed description of the environment is used in RAM and LYBIN. The results in this thesis indicate that RAM is the best choice for a propagation model, as it handles multipath and dipole effects which become significant at low frequencies and long ranges. The method is applied to measurement data acquired in the Oslofjord, with source level estimates for seven commercial ships obtained and discussed.

Sammendrag

Skipsstøy i havet grunnet kommersiell skipsfart har fått økt interesse de siste årene på grunn av den potensielle påvirkningen av marint liv og havmiljø. Derfor har raske metoder for å estimere kildenivået av kommersielle skip oppnådd betydelig forskningsinteresse. Selv om flere målestandarder finnes som beskriver måleprosedyrer i dedikerte måleområder eller under kontrollerte forhold, er det interesse for metoder tilpasset for mindre ideelle måleforhold, slik som i trange fjorder med betydelig skipsfarts aktivitet. Denne masteroppgaven tar for seg et slikt mindre ideelt oppsett i sammenheng med måling av skipsstøy med en hydrofon nær havbunnen i grunt vann med skipspasseringer ved lange avstander (flere ganger vanndybden).

En metode for kildenivåestimering av skipsstøy er formulert som justerer målt (mottatt) nivå for bakgrunnstøy, bruker et avstandsestimat basert på data fra et automatisk identifikasjonssystem (AIS) for skip, og korrigerer for propagasjonseffekter ved hjelp av en kompleks akustisk propagasjonsmodell (RAM) med en distribuert kildemodell. I tillegg er propagasjonsmodellen LYBIN og enkel sfærisk sprednings-tap korrigert med som alternativer. Målet er monopole kildenivåer i 1 Hz bånd og 1/3 oktav frekvensbånd. En detaljert beskrivelse av undervannsmiljøet er brukt i RAM og LYBIN. Resultatet i denne oppgaven indikerer at RAM er det beste valget for en propagasjonsmodell, ettersom den tar hensyn til flerveis- og dipol-effekter som blir betydelige ved lave frekvenser og lange avstander. Metoden er brukt på måledata fra Oslofjorden, hvor kildenivåestimater for syv kommersielle skip er funnet og diskutert.

Preface

This thesis concludes my Master of Science degree in Electronics at the Norwegian University of Science and Technology. The work has been carried out at the Department of Electronics and Telecommunications.

The assignment was given by FFI (Norwegian Defence Research Establishment), which has provided all the necessary data and information to conduct the research done in this thesis.

I would like to thank my supervisor Hefeng Dong for help, guidance and encouragement with my thesis work. I would also like to thank my co-supervisor Dag Tollefsen at FFI very much for his help and guidance with the thesis, and for contributing to resolve problems as they arose. Thanks are also directed to the other employees at FFI who have been helpful in providing data, and to Alexios-Georgios Korakas who has helped me with the Range dependent Acoustical Model. I would also like to thank friends and family for support.

Contents

Chapter 1

Introduction

Underwater noise from marine vessels have gained attention in recent years, especially within the EU. In the context of gaining a better understanding of how underwater noise affects the environment and managing noise exposure, it is first important to establish how much noise marine vessels produce. Well defined measurement methods are necessary to get consistency within noise source level measurements of marine vessels.

A standard describing procedures for measurement of underwater sound from ships was approved by the American National Standards Institute (ANSI) in 2009. While the standard applies to an ideal measurement set up, a situation where a hydrophone is placed near the seabed to measure noise at longer ranges requires adjustments to the method described in the standard. Such adjustments will be formulated as a method and implemented, based on results from the project thesis [1]. The method will be tested on a dataset containing acoustic recordings of vessels of opportunity.

Chapter 2

Theory

2.1 Signal processing

This section will describe which signal processing steps are required to achieve the wanted source level with the correct units, and why they are chosen.

An acoustic measurement system typically gives a discrete time signal at the end of the signal chain. This signal has then been amplified and sampled through an analog to digital (A/D) converter. To get the right unit for the signal one must adjust the amplitude with the hydrophone sensitivity, or an overall system gain which is usually frequency dependent. Then the signal is analyzed in the frequency domain, and the source level is estimated in a discrete continuous spectrum or in 1/3 octave bands.

2.1.1 Fourier transform

Take an analog signal $x_a(t)$, sampled at a rate $F_s = \frac{1}{\Delta t}$ samples per second, resulting in sampled signal $x_a(n\Delta t) \equiv x(n)$. The Discrete Fourier transform (DFT) of the discrete-time finite energy signal $x(n)$ of length N can be defined as [2]

$$X(k) = \frac{1}{N} \sum_{n=0}^{N-1} x(n) \exp(-i2\pi nk/N) \qquad n, k = 0, ..., N-1 \tag{2.1}$$

where

$$k = \frac{f}{\Delta f}. \tag{2.2}$$

Here Δf is the frequency resolution or the size of the frequency bin,

$$\Delta f = \frac{F_s}{N}. \tag{2.3}$$

The length of the signal in seconds is

$$T = \frac{N}{F_s} = \frac{1}{\Delta f}. \tag{2.4}$$

Note that Eq. (2.1) differs from the Fast Fourier transform (FFT) function in MATLAB by the factor $1/N$.

2.1.2 Power spectral density

The true power spectral density, $\Gamma(f)$, of a random stationary process without finite energy is defined in [3] through the autocorrelation function

$$\gamma(\tau) = E[x_a^*(t) \cdot x_a(t+\tau)], \tag{2.5}$$

and its Fourier transform via the Wiener-Khintchine theorem as

$$\Gamma(f) = \int_{-\infty}^{\infty} \gamma(\tau) \exp(-i2\pi f\tau) d\tau. \tag{2.6}$$

However, in practice, $\Gamma(f)$ is estimated through a finite duration signal. Through the Fourier transform in Eq. (2.1) one can estimate the sampled power spectral density (PSD) of the signal, defined in [2] and [4] as

$$\begin{aligned} \mathrm{PSD}(k) &= 2\frac{|X(k)|^2}{\Delta f} \\ &= \frac{2}{F_s N} \left| \sum_{n=0}^{N-1} x(n) \exp(-i2\pi nk/N) \right|^2 \qquad n, k = 0, ..., N-1 \end{aligned} \tag{2.7}$$

A factor of 2 in Eq. (2.7) is included to preserve the total power as one normally uses the one-sided spectrum of a real signal. If the signal $x(n)$ has unit pascal (Pa), then the PSD(k) has unit pascal squared pr hertz (Pa^2/Hz). The PSD shows how the power of the signal is distributed over the frequencies. This is similar to the periodogram in [3, p. 969], but with a different normalization constant.

When the PSD is estimated for a time segment, often a short duration of the segment is used, e.g. 1 second, and the PSD is found for several succeeding or overlapping time windows and then averaged. This technique is known as the method of averaged periodograms. The reason for averaging the PSD is to reduce the variance in the estimate [3, p. 975]. The reduced variance comes with the cost of reduced frequency resolution as the signal length is reduced, ref. Eq. (2.3).

The total power (P) of the signal is

$$P = \sum_k \mathrm{PSD}(k)\Delta f. \tag{2.8}$$

A property of the sampled estimate of the PSD in Eq. (2.7), is that the level of each sample is dependent on the size of the frequency bin, Δf, as is evident from the formula for power, Eq. (2.8). The power of a signal calculated with different sizes of the frequency bin will be the same, but the PSD with the smaller Δf will have levels higher than a PSD with a larger Δf. To ensure a consistent representation of the PSD, one can normalize the PSD to the levels of a PSD with a 1 Hz frequency bin. The PSD in 1 Hz bins is then

$$\mathrm{PSD}_{1\mathrm{Hz}} = \mathrm{PSD}\frac{\Delta f}{1\ \mathrm{Hz}}. \tag{2.9}$$

Here $\frac{\Delta f}{1\ \mathrm{Hz}}$ is a dimensionless constant, and Δf is the size of the frequency bin used in the analysis.

2.1.3 Window functions

One can also multiply the time segments by a window function, so that the start and end of the segments are attenuated and the discontinuities at the endpoints are removed, thus reducing spectral leakage [3]. Indirectly, a rectangular shaped window is applied if no other window is used. Another window, like the Hanning window, has lower side-lobes in the spectrum (less spectral leakage) but a wider main-lobe width than the rectangular window. By applying a window function, there will be a trade-off between main-lobe width and spectral leakage. The main-lobe width of the window spectrum controls the ability to distinguish between two close spectral components. This is the second factor that affect the frequency resolution in addition to the size of the frequency bin in Eq. (2.3). When the DFT length is the same as the signal length, these two factors limit the frequency resolution with about the same amount [5].

If a signal-segment of length T=1 s is used, the size of the frequency bin is, according to Eqs. (2.3) and (2.4), 1 Hz. If a Hanning window is applied prior to the DFT, the frequency resolution (main-lobe width at -3dB) is approx. 1.4 Hz, and the highest side-lobe is -31.5 dB according to [4].

Another factor to consider is the maximum amplitude error, explained by [4] as ”the maximal possible error in the estimation of the amplitude of a sinusoidal signal that may fall anywhere within one frequency bin.” This error is -3.9 dB for a rectangular window, and -1.4 dB for a Hanning window.

The method of averaging the PSDs with or without overlap, and with a window function is called the Welch Method of averaging modified periodograms [3].

If the window function is $w(n), n = 0, ..., N-1$, one can define an incoherent gain (normalization) factor for the window function as

$$G_{\mathrm{INC}} = \frac{1}{N}\sum_{n=0}^{N-1} w^2(n). \tag{2.10}$$

The total signal $x(n)$ of length M can be divided into L different overlapping segments of length N,

$$x_j(n) = x(n + jD), \quad \begin{array}{c} n = 0, 1, ..., N-1 \\ j = 0, 1, ..., L-1 \end{array} \tag{2.11}$$

where jD is the starting index for the jth segment. If $D = N$, there is no overlap. If $D = N/2$, there is 50% overlap, and $L = 2M/N - 1$, as the last window will be partly outside the domain.

The formula for the modified PSD for one segment, j, is then

$$\begin{aligned} \mathrm{PSD}_j(k) &= 2\frac{|X_{w,j}(k)|^2}{\Delta f G_{\mathrm{INC}}} \\ &= \frac{2}{F_s N G_{\mathrm{INC}}} \left| \sum_{n=0}^{N-1} x_j(n) w(n) \exp(-i2\pi nk/N) \right|^2, \qquad n, k = 0, ..., N-1 \end{aligned} \tag{2.12}$$

where $X_{w,j}(k)$ represents the Fourier transform of the segment j multiplied by a window function. The averaged modified PSD is then

$$\mathrm{PSD}(k) = \frac{1}{L} \sum_{j=0}^{L-1} \mathrm{PSD}_j(k). \tag{2.13}$$

2.1.4 1/3 Octave Bands

To get the spectrum in 1/3 octave bands, it is normal to use bandpass filters and then calculate the root mean square (RMS) value for each band. However, when the PSD is available, it is possible to take the average of the PSD within the frequency bins of each band to get the levels in $\mu\mathrm{Pa}^2/\mathrm{Hz}$.

The exact center frequencies for 1/3 octave bands ranging from 10 Hz to 3 kHz, can be found as

$$f_{\mathrm{n,center}} = 10^{n/10} \qquad n = 10, ..., 35. \tag{2.14}$$

The lower and upper frequency band limits are found from

$$\begin{array}{rl} f_{\mathrm{n,max}} = & f_{\mathrm{n,center}} 2^{1/6} \\ f_{\mathrm{n,min}} = & f_{\mathrm{n,center}} 2^{-1/6} \end{array} \quad n = 10, ..., 35. \tag{2.15}$$

The "preferred" center frequencies are slightly rounded compared to the exact center frequencies [2].

The average PSD in a 1/3 octave band n is then (using the PSD(k) in Eq. (2.13))

$$\mathrm{PSD}_{\mathrm{octave}}(n) = \frac{\sum_{k=k_{min}}^{k_{max}} \mathrm{PSD}(k)}{k_{min} - k_{max} + 1}. \tag{2.16}$$

Here k_{min} and k_{max} is found from Eq. (2.2) and Eq. (2.15) for the specific frequency limits of band n. This gives a unit of $\mathrm{Pa}^2/\mathrm{Hz}$.

2.1.5 Broadband Source Level

Another useful measure of the source level, is the broadband source level (BSL), here defined as the sum of the source level from 20 Hz to 1 kHz, as used by [6]. Here it is assumed that the source level is as defined in Eq. (2.18), that is, the PSD adjusted for transmission loss. The indexes k_{min} and k_{max} correspond to 20 Hz and 1 kHz respectively, and are found from Eq. (2.2).

$$BSL = \sum_{k=k_{min}}^{k_{max}} \mathrm{SL}(k)\Delta f. \tag{2.17}$$

The formula can be applied in an analogous way to get the broadband received level (BRL).

2.2 General source level measurement

This section will describe how the source level of a surface vessel may be measured.

Source level measurement is preferably done in an ideal setting (see section A) [7]. This is difficult to achieve in practice, as there often is elements in the environment or measurement system that is undesirable.

The measurement of a vessels source level must be done in the far-field and not in the near-field. In the near-field the sound may vary rapidly and not be representative for the sound far away from the source. As a rule of thumb, the distance from the source must be greater than ten times the acoustic wavelength to be in the far-field. The far-field source level is then used to calculate the source level at 1 m distance from the source. However, the measurement should be close enough to ignore propagation effects (other than geometrical spreading). These two requirements are in conflict when a surface vessel is considered, as the far-field contains a surface reflected contribution. Ainslie [8] describes two general methods for far-field measurements.

The first method is the "monopole method," and it is the one used in this thesis. Here a monopole source at some depth is assumed, and the transmission loss (TL) according to this geometry is estimated. The source level (SL, in dB values) is then acquired from the measured (received) sound pressure level (SPL) according to

$$\mathrm{SL}^{\mathrm{mp}} = \mathrm{SPL} + \mathrm{TL}. \tag{2.18}$$

This method is sensitive to source depth and the TL model, but the resulting monopole source level ($\mathrm{SL}^{\mathrm{mp}}$) is independent of the measurement environment.

The other method is the "dipole method." Here the contribution from the surface reflection is included in the source level, which means that the source is modeled as a dipole. The only correction applied to the SPL is the spherical spreading law.

$$\mathrm{SL}^{\mathrm{dp}} = \mathrm{SPL} + 20\log_{10}(r/r_{\mathrm{ref}}). \tag{2.19}$$

Here r is the distance from the acoustic center of the ship to the receiver, and r_{ref} is a reference distance, normally 1 m. An approximate relationship between the dipole source level $\mathrm{SL}^{\mathrm{dp}}$ and the monopole source level $\mathrm{SL}^{\mathrm{mp}}$ is given as (ref. [8] Eq. (8.190))

$$\mathrm{SL}^{\mathrm{mp}} \approx \mathrm{SL}^{\mathrm{dp}} + 10\log_{10}(\frac{1}{2} + \frac{1}{4k^2 d_s^2}), \tag{2.20}$$

where k is the wave number and d_s is the source depth. This dipole source level is often referred to as an affected source level, as it does not take surface reflection, bottom reflection or absorption into account. The ANSI standard [7] described in A proposes this source level.

Transmission loss is defined in [8] as "the ratio in decibels between the acoustic intensity $I(r,z)$ at a field point and the intensity I_0 at 1-m distance from the source." The intensity of a wave is proportional to the square of the pressure, and one can thus write

$$\begin{aligned} \mathrm{TL} &= -10\log_{10}\frac{I(r,z)}{I_0}, \\ &= -20\log_{10}\frac{|p(r,z)|}{|p_0|} \qquad \text{(dB re 1m)}. \end{aligned} \tag{2.21}$$

TL can be seen as the sum of loss due to geometrical spreading and loss due to attenuations in the medium. In Eq. (2.19) for the dipole method, the only loss mechanism considered is geometrical spreading. For an omni-directional source in space without loss, the intensity spread equally around the sphere is inversely proportional to the range squared, $I \propto \frac{1}{4\pi r^2}$. Inserting this in Eq. (2.21), one gets $TL = 20\log(r)$ for spherical spreading.

One must be aware of how the source level is defined, and how the environment is described when comparing source levels, as different definitions can give different source levels. As mentioned, the true monopole source level is the goal of this work, such that the method can give consistent results for various environments.

Chapter 3

Methods

3.1 Measurements

In the project work [1], a method for measurement of surface vessel ship noise in the far-field from a sensor on the seabed was formulated. This method was based on the ANSI standard [7] (ref. A), with the main difference being the measurement of the monopole source level instead of the dipole source level. This implied the need for a more complex model for the TL than a model based on spherical spreading, as described in section 2.2. This is the method that the source level measurement will be based on in this thesis.

Now the measurement method will be described.

It was found in [1] that the TL estimation should take into account bottom and surface reflection, refraction and surface wind. Accordingly, a sound speed profile (SSP), a bottom bathymetry and bottom properties should be given as input to a TL model. The propagation model LYBIN has been shown to satisfy the necessary requirements, but is an incoherent model (i.e., it does not sum propagation paths coherently and does not account for phase shifts associated with reflection from boundaries). This results in an TL with little frequency dependence. It was proposed in [1] to use another model which is coherent, and the Range-dependent Acoustic Model (RAM) [9] is such a model. In addition to the TL estimation requirements, the vertically distributed source model (ref. section 3.3) should be implemented as described in [1], and this is also possible with RAM. The reason for using the vertically distributed source model is that the coherent effects present in the TL from RAM may have stronger variations than in the real case where the wave field may be more diffuse; also, the model is assumed to give a more realistic representation of ship noise than a point source [10]. The model is described further in section 3.3. To evaluate these models, the monopole SL with TL from both LYBIN and RAM will be presented along with the dipole SL with spherical

spreading TL.

As the recording hydrophone used in this thesis is bottom mounted (see chapter 4) and the distance to the ships may be long, the measurement geometry set by the ANSI standard (ref. A) is slightly modified. The data window length (DWL, ref section A.3) is set to be the greater of the ship length or 100 m, and is not dependent on the distance between the ship and hydrophone at the closest point of approach (CPA). If it was, the data window could be long and contain noise contributions from other sources. By setting a shorter data window, possible contributions from other sources are minimized.

A key element in the method is that the distance and location of the CPA is determined from AIS (Automatic Identification System) data containing GPS information on ships in the area [11]. According to the standard, the data window used for analysis should be centered on the acoustic center (horizontally) of the ship, which could be defined as halfway between the engine room and the propeller, or as the location of the maximum broadband output. The data window used in this thesis is centered on the CPA (referenced by the GPS antenna location) of the ship and will give the broadside source level of the ship. For cases where a measurement of the broadside of the ship at CPA is not available or usable for any reason, the alternative of measuring the SL before CPA and after CPA, and then take the average value of those as the resulting SL has been used. This will though not be a broadside measurement, but an approximation.

A measurement of the background noise is used to verify that the measurement of the ship noise has an acceptable signal (with noise) to noise ratio (SNR). If the SNR is less than 10 dB and more than 3 dB, adjustments are applied according to Eq. (A.4). For an SNR below 3 dB, it is adjusted as if the SNR is 3 dB and marked as such. The standard recommends adjustments in 1/3 octave bands, not in discrete frequency components, however, here adjusted levels will be presented in discrete frequencies as well.

The background noise is estimated for some time (10-30 min) before or after the ships CPA, where the intensity seems lowest. With high vessel traffic, this is necessary to get the present ambient noise image. This may introduce a problem as the background noise can contain an attenuated version of the ship noise, and thus not be a good indicator for the ambient noise level. However, the problem must be assessed and the measured background noise evaluated for each case.

The resulting received and source level shall be in a spectrum of 1 Hz bands, and in 1/3 octave bands, in the frequency range 10 Hz to 3 kHz (limited by measurement equipment). The received level is the sound level that is measured by the hydrophone, and the source level is the estimated sound pressure level at 1 m from the source. The RL and SL is found as power spectrum densities with unit dB re $1\mu\text{Pa}^2/\text{Hz}$ and dB re $1\mu\text{Pa}^2/\text{Hz}$ at 1 meter respectively, as described in section 2.1. The steps in the algorithm to get the RL and SL is shown in Figure 3.1 and 3.2 respectively. The recorded signal of the ship at the relevant time is split into segments. For each segment the PSD is calculated and an overall system gain is

added. For the SL the TL for each segment is added. Then the PSDs are averaged and the levels are adjusted if the SNR is below requirements.

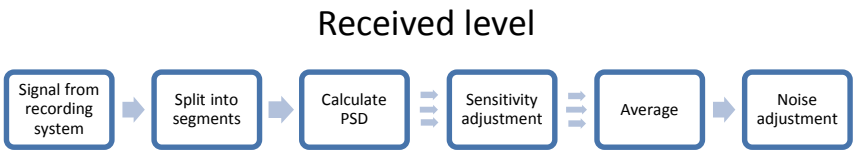

Figure 3.1: Steps in the signal processing algorithm used to get the RL.

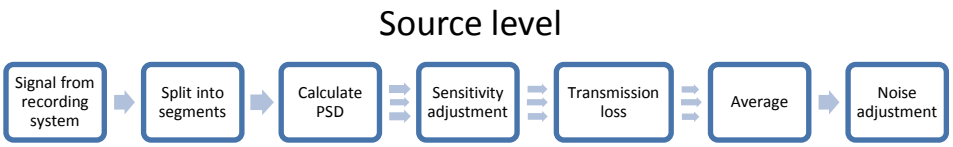

Figure 3.2: Steps in the signal processing algorithm used to get the SL. The difference from the RL, is that here the TL is included.

3.2 Transmission loss corrections

The main purpose of this thesis is to use propagation models to estimate a TL for specific environments. Here the two models LYBIN and RAM will be described.

3.2.1 LYBIN

The acoustic ray trace model LYBIN is one model that will be used to estimate transmission loss. It is owned by the Norwegian Defence Logistic Organisation (FLO) and maintained by FFI (Norwegian Defence Research Establishment). According to [12], LYBIN has been "proven with measurements, and has prediction accuracy similar to other acknowledged acoustical models."

Ray theory assumes that sound propagates along rays that are normal to wave fronts. In a medium where the sound speed is constant, the rays will follow straight lines, but when the sound speed changes the ray paths are curved. Ray tracing is a method that calculates the trajectories of the sound from a source at given angles. The transmission loss can then be found coherently or incoherently depending on implementation, based on the curvature and length of the ray. LYBIN is incoherent.

Ray tracing is a high-frequency approximation, that is, the sound speed should vary negligibly over a length corresponding to the longest wavelength. Another

approximation is that the spatial variation of the amplitude must be small. At the edges of the sound field, the variation is normally high, so diffraction effects are not shown well in ray tracing.

The propagation path can be determined from knowledge of how the sound speed varies with depth. It is normal to assume that the speed is homogeneous with regards to range, but it is possible to include range dependent data depending on implementation of the ray tracing theory. E.g LYBIN has this functionality. The sound speed variation with depth is called the sound speed profile (SSP), and there is two main variants of variation, increase and decrease of sound speed with increasing depth. When the SSP is more complex, one generally divides the SSP into thin layers where the profile is linearized, and then the rays may be computed numerically. For a more thorough and mathematical formulation of ray tracing, see [13].

LYBIN has capability of including a bottom profile with a predefined bottom class (or reflection coefficient). It also has an option for including wind speed or wave height to model more realistic surface interactions. LYBIN also includes thermal absorption in the transmission loss. However, absorption is not so important, as this loss is in the order of 0.1 dB/km for the highest relevant frequencies according to [13]. At 5 km, the absorption loss is about 0.5 dB for 3 kHz. All this makes LYBIN able to predict the acoustic field in a complex environment.

The number of rays used in the calculations in this thesis is 75000, with 500 range cells and 250 depth cells. The source beam-width is set to 360 degrees vertically, corresponding to a omnidirectional point source, with the sonar in passive mode.

3.2.2 RAM

An other model that will be used in transmission loss estimation is RAM, or Range dependent Acoustical Model. It is based on a parabolic equation method, and written by Michael D. Collins [9]. The code is written in FORTRAN, and is based on the split step Padé solution which is the most efficient parabolic equation method according to [9]. The model is coherent, a far-field approximation, and handles range dependent environments by treating them as a sequence of range-independent environments, such as sound speed in water and bottom profiles.

In its calculation, RAM includes information about the bottom as density, sound speed, attenuation and depth. Bathymetry points are linearly interpolated in range in RAM according to the current range step, but the bottom profiles are interpolated and smoothed before they are given as input to RAM. The same is true for SSPs, which also are interpolated and smoothed beforehand.

RAM is an accurate model provided that the inputs are selected properly, such as the grid spacing, the depth of the computational domain and thickness of the absorbing layer (needed to dampen waves reflected from the lower boundary of the

Table 3.1: Chosen parameter values in RAM for different frequencies. The wavelength is λ=1480/frequency. dr and dz are the range and depth step respectively. Zmax is the depth of the computational domain where zb is the deepest point of the bottom profile.

Frequency	$<$ 100 Hz	$<$ 1 kHz	$<$ 4 kHz
dr [m]	$\lambda/12$	$\lambda/6$	$\lambda/6$
dz [m]	dr/5	dr/4	dr/4
Abs. layer [m]	10λ	15λ	25λ
Zmax [m]	50λ+zb	50λ+zb	75λ+zb

computational domain). Convergence tests can be performed to verify the accuracy, so that the parameters are selected appropriately. As these parameters are strongly dependent on the wavelength, such convergence tests are time consuming when the calculations shall be made for a large range of frequencies (10 Hz to 3 kHz). Therefore, the depth and range grid spacing, the depth of the computational domain and the thickness of the absorbing layer are selected according to chosen frequency bands. Simple tests have been made to verify that the parameters give acceptable results. The grid parameters in RAM can be seen in Table 3.1. The number of grid points increases with frequency, and the number of Padé terms used in the rational approximation was three. More tuning of the parameters to reduce the run-time is possible, but that was not prioritized.

3.3 Source model

In TL estimation, especially when the TL model is coherent, the depth of the source has a large influence on the result. Here the source depth of ships will be discussed, and a model to approximate the distributed nature of a ships source radiation will be presented.

A surface vessel radiates noise in a complex way. The propeller is considered to be the main acoustic source at lower frequencies, connected to the fundamental blade rate and its harmonics, together with broadband cavitation noise [10]. In addition, the main and auxiliary engines and the gearing is coupled to the hull and make it vibrate.

In TL estimation, a source depth must be determined to correctly model the interference between a wave reflected by the surface and the direct wave, a coherent effect called the Lloyd's mirror (LM) effect [1] (see also section B). The source depth of a vessel is not trivial to determine. However, it is possible to assume an effective source depth. Such an effective source depth (d_m) can according to [14] and [10] be estimated as

$$d_m = D - 0.85P, \tag{3.1}$$

where D is the ship draft (maximum depth of the ships hull in the water) and

P is the diameter of the ships propeller. This point source model is based on an assumption that the upper part of the propeller is the main cavitation source.

According to [15], a modification to the point source model gives a better match to observed LM patterns. The basis for this model is the same as for the point source. However, now the source is not modeled by a point, but with a source that is Gaussian distributed vertically in depth. This model will now be described as follows.

One can start with an expression for the direct pressure wave at a horizontal range r and depth d_r,

$$p = \left(\frac{\exp(i2\pi f r_d/c)}{r_d} \right). \tag{3.2}$$

where the traveled distance for the wave can be written in terms of the depth of the source, d, and receiver, d_r, and the horizontal range r between them:

$$r_d = \sqrt{(d_r - d)^2 + r^2}. \tag{3.3}$$

One can then modify this by integrating it over a weighting function, which is Gaussian distributed [10]. The weighting function is

$$W(d) = (\sigma\sqrt{2\pi})^{-1} \exp\left(\frac{-(d - d_m)^2}{2\sigma^2} \right), \tag{3.4}$$

where d is the depth variable in meters, σ is the standard variation of the source depth in meters, d_m is the mean source depth in meters, or the effective source depth.

The equation for the sound pressure level with a distributed source is then

$$L_{p,G} = 10 \log_{10} \left[\int_0^D p(d)^2 \frac{W(d)}{\gamma} \mathrm{d}d \right]. \tag{3.5}$$

The integral over depth d is from the surface to the depth of the draft D. The constant γ have been applied to Eq. (3.5) to normalize the contribution from $W(d)$, and is found as

$$\gamma = \int_0^D W(d)\mathrm{d}d = \int_0^D (\sigma\sqrt{2\pi})^{-1} \exp\left(\frac{-(d - d_m)^2}{2\sigma^2} \right) \mathrm{d}d. \tag{3.6}$$

An example of the weighting function with parameters used for the ship Thebe (described later in the thesis) can be seen in Figure 3.3.

If one have the TL in dB for different source depths, one can use Eq. (3.5) with

$$p(d) = 10^{-TL(d)/10}, \tag{3.7}$$

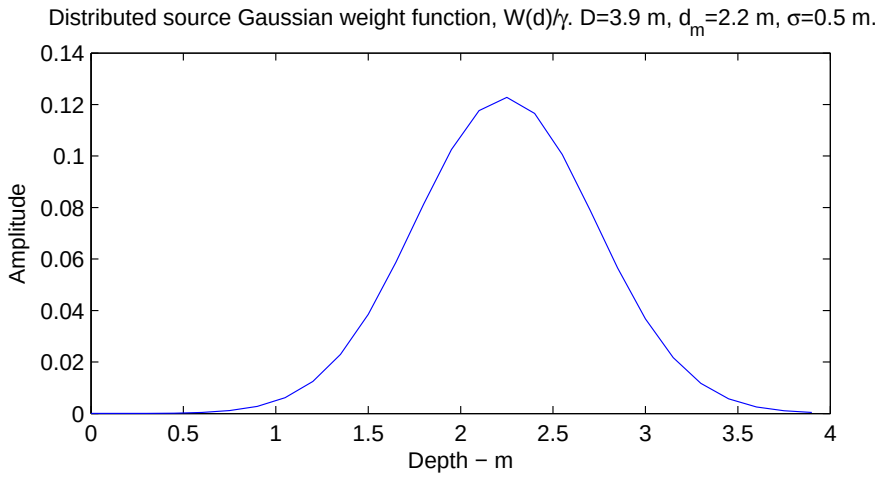

Figure 3.3: A plot of the normalized Gaussian distributed weight function used in the distributed source model for the ship Thebe. The parameters used are D=3.9 m, d_m=2.2 m and σ=0.5 m. The discretization step of the depth variable d is 0.15 meter.

and approximate the integral as a sum.

The distributed source model may not give the exact interference pattern for a vessel, as σ and the source depth generally are unknown, and have to be set based on the draft of the vessel. As described, one can assume an effective source depth. This again requires knowledge of the propeller. In a measurement of a variety of merchant ships [16], a source depth of 6 m was chosen to be representative to the class of merchant ships, and used to calculate the TL spectrum. It is also stated that other choices of source depth, like the propeller depth, could yield different results. Two source depths were used by [6] to estimate the TL; 7 m and 14 m, which is stated to be typical depths of ship propellers. In that case the TL from a parabolic equation model was used to argue that the spherical spreading law as appropriate to account for the TL at the relatively deep-water site. Obviously, it is a challenge to set a specific depth for the source. If no information about the propeller is available, a provisional method may be to set the propeller diameter to half the draft, which would be correct for the ships referred to in [10] and [15]. Also σ is connected to the propeller, as it represents the cavitation volume of the propeller. A source depth standard deviation of one quarter of the propeller diameter is used by [15]. Normally, the higher capacity a vessel operates at, the more the propeller cavitates causing more broadband noise.

Thus the propeller diameter can be set as half the draft,

$$P = \frac{D}{2}, \tag{3.8}$$

and the standard deviation as a quarter of the propeller diameter

$$\sigma = \frac{P}{4}. \tag{3.9}$$

An example of an analytical TL showing the LM effect with and without a distributed source can be seen in Figure 5.13 in section 5.3.1.

Chapter 4

NGAS10 data

This chapter describes the dataset that will be used in the analysis, including the equipment, the ship recordings, location data and environment information. Most of the information given here is taken from [17].

4.1 The sea trials

The gear used to record the ship noise is a NILUS (Networked Intelligent Underwater Sensor) node. This is a tripod construction unit composed of hydrophones, magnetic sensors, an acoustic modem and a flotation device. The node is placed on the sea floor and can be easily deployed and recovered. During the NGAS (Next Generation Autonomous Systems) sea trials in Horten in 2010, four NILUS nodes were deployed several times during a 3-week period. The purpose of the trials were to test an underwater sensor and communication system, and the acoustic sensors were recording most of the time. These recordings are the basis of the measurement data studied in this thesis. The location of the NILUS nodes can be seen in Figure 4.1. Only two of the nodes had acoustic sensors with specifications suitable for ship noise measurement (DIFAR-sensor), and during the trials, all four node locations (ref. Fig 4.1) were used by these two nodes. The depth and location of each of the nodes are listed in Table 4.1.

Table 4.1: Depth and location of the four NILUS nodes [17].

NILUS location	Depth [m]	Latitude	Longitude
A	195	59N 28.363	10E 29.142
B	38	59N 28.752	10E 30.049
C	108	59N 28.035	10E 29.850
D	44	59N 27.512	10E 27.929

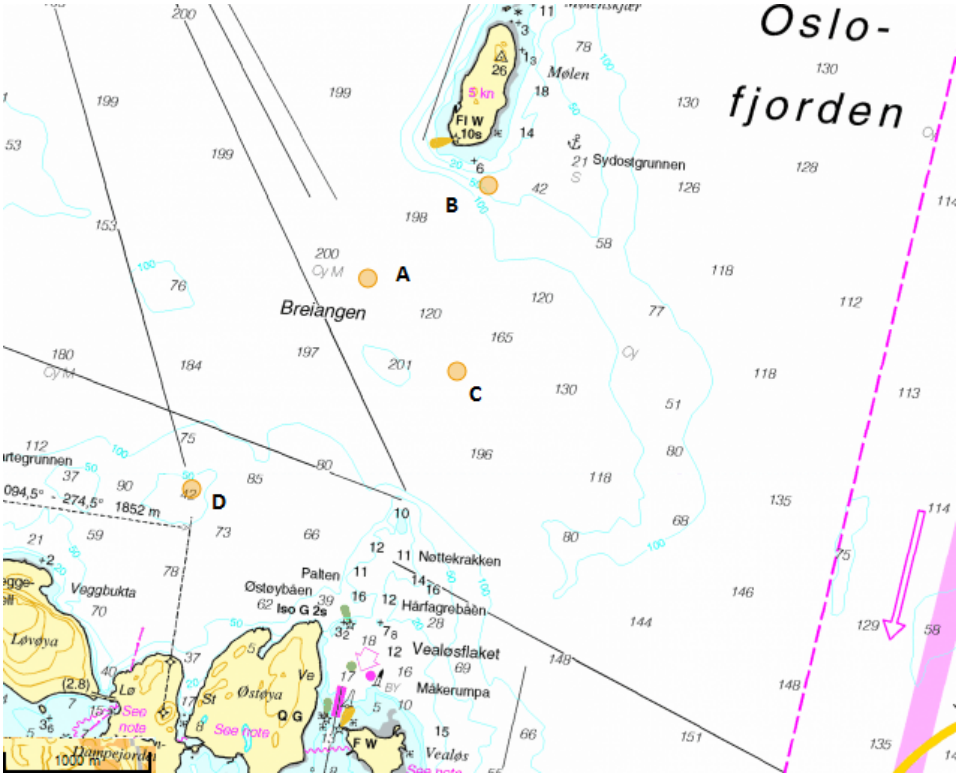

Figure 4.1: A map of Breiangen outside Horten with the location of the NILUS nodes A, B, C and D. Taken from Kartverket.

4.2 Acoustic sensors

The acoustic sensor used by two of the nodes is a DIFAR-sensor (Directional frequency analysis and recording), where the omni-directional channel is used. This sensor has a known frequency response which is used in the signal processing [18], and the usable frequency range is from 10 Hz to 3 kHz, which is the range the SL results will be presented in. The sensitivity is 122 dB ±3 dB re 1 μPa at 100 Hz (factory specification [19]). The acoustic data are recorded to a memory card with a 24-bit A/D-converter and a sampling frequency of 18 kHz. The data is later converted to 16-bit wav files and decimated to 9 kHz.

There was a problem with an internal amplifier that was saturated when the acoustic modem of the NILUS-node was transmitting. This caused the recorded signal to be corrupted at the time of these transmissions, which occurred sporadically throughout the recording. In addition, there seems to be some sort of amplitude clipping of the recorded signal at high intensities. At the ships CPA, the received pressure level is normally high, and the recording of ships passing at a distance

shorter than 500-700 m seems to experience such clipping. These two effects render some of the recorded ship passings unsuitable.

On the NILUS-node a Scan-Sense pressure sensor of type PS2091-001 (PS-2000 series) is mounted. This pressure sensor is used to measure the current depth which is then logged. The sensor is very accurate, but has not been calibrated, and may thus give a depth within ±3 meters of the true depth, according to the NILUS hardware documentation. During trials the reported depth is corresponding with echo-sounders and charts.

4.3 Acoustic data

In the project work [1], data from the NILUS-location B was considered best suited for analysis, based on bottom profiles and distance to passing ships going to and from Oslo. For ships going to Drammen, all node locations were deemed usable. To find usable ship passings, GPS information from the AIS data recorded during the trial was used.

As described in the method, there must be a sufficient time before and after a ship passing where no other ships are in the near vicinity, to ensure a measurement uninfluenced by other ships. This proved to be a difficult criterion to fulfill, as there was a lot of activity in the fjord. The background noise between ship passings was generally high. Sometimes the levels during a passing did not rise significantly above the levels before and after the passing should have occurred according to the AIS data. This may be caused by other smaller vessels, e.g fishing boats or shrimp-trawlers, operating in the area that is not using the AIS system. The combination of background noise and amplitude clipping (only low intensity recordings could be used) resulted in low SNR for many of the passings, making them unsuitable for source level estimation. A total of about 50 hours of acoustic data was recorded during the 3-week period.

4.3.1 Suitable recordings of ship passings

Only a few passings during the trails proved to satisfy conditions necessary to estimate the broadside source level in a satisfactory way. The conditions included minimal observable amplitude clipping, high enough SNR, and enough time between passings.

The passing of the cargo ship Thebe the 10th of June was recorded at both NILUS location C and D coming from Drammen going south-east. The recording at NILUS-C was good with little detectable interference from other ships. However, there may be interference from other unidentified ships in the recording at NILUS-D, but it will still be analyzed to see if the SLs are comparable.

4.3.2 Less suitable recordings of ship passings

As only the two passings by ”Thebe” was found to be satisfied by the conditions, it was decided to widen the criteria to get more results. There were a few passings that satisfied the conditions except for the observable amplitude clipping. The RL and SL of these passings will be estimated as the dB average of a measurement just before and just after the observable amplitude clipping. This will mostly avoid the distorted signal and still gain a reasonable SNR. This will however introduce another uncertainty to the resulting source level, as the noise radiated from an angle near beam or stern of the ship tend to be lower than the broadside radiated noise [10].

The relevant ships that will be analyzed are Elektron II, Autobank and Wilson Husum. Autobank and Wilson Husum were recorded at NILUS-C and NILUS-D. The amplitude clipping occurred at NILUS-C as it was closest. There may be interference from other unidentified vessels at NILUS-D for both the ships, but they will still be analyzed so they can be compared to the results from NILUS-C.

The passings of Thebe, Elektron II, Autobank and Wilson Husum were all recorded at the 10th of June.

4.4 AIS data

During the trail, about 192 ships transiting in the Oslo fjord near Horten were tracked by the AIS. The AIS data needed to be parsed and processed to give the wanted information. A parser by Høgskolen i Ålesund [20] was used in addition to scripts written by FFI to filter out ships that were not moving and create a list of all the ships transiting the area of interest, stating the time and the distance to each node location at CPA. In addition, the scripts were altered to also output the length, breadth, draft, location of the GPS antenna and the accuracy of the GPS data for each ship.

The AIS messages containing information about the draft of the ship did not have a time stamp. Within the time window of the trail a ship may be recorded with several drafts, as it may have loaded or unloaded cargo during this time. For this reason, the draft used to estimate the source depth is an average of the reported drafts for a ship.

Ships send position messages at intervals of up to 10 seconds [11], and even fewer may be recorded by the AIS receiver. This leads to a possible source of error for estimation of time and location at CPA between a NILUS-node and a ship. Therefore, for the relevant ships, the GPS coordinates with time stamps of each track are interpolated to every 1 second. In Figure 4.2 the tracks of the four ships that are analyzed are shown. The track of Elektron II clearly shows the need for interpolation of the GPS data.

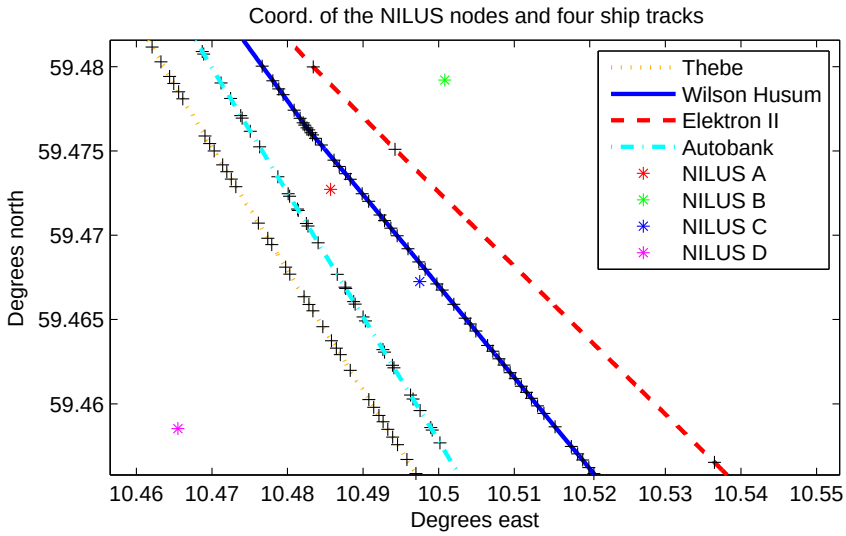

Figure 4.2: Tracks of the four ships that are analyzed. The plus marks show the original GPS coordinates which have been interpolated to create the tracks. Also the location of the NILUS-nodes is shown.

4.5 Environment data

Here the data regarding the environment will be shown, such as wind, rain, temperature, relevant sound speed profiles and bottom properties.

A plot of the wind, rain and temperature during the month of June can be seen in Figure 4.3 [17]. The wind speed during the 10th of June was mostly around 4 m/s, and there was also no rain according to the measurements in Figure 4.3. This indicates calm weather that should not influence the measurement noticeably.

There were taken SSP measurements at several times and locations during the trials using a CTD (conductivity, temperature, depth) probe of type SD204 from Saiv Instruments [17]. In Figure 4.4 the SSPs have been plotted as sound speed vs depth. Some of the SSPs were taken at shallow and deep water, however, they are very similar at the overlapping depths. This indicates a horizontally homogeneous water column throughout the area. There are some variation in the upper layer probably due to changes in weather conditions. In the period June 7th-16th a strong sound propagation channel at 30-40 m depth was present.

The most relevant SSP is 09-A, seen in Figure 4.4. The location of the measurement is in the area of the NILUS-locations, and taken only one day before the relevant ship passings (described in section 4.3). When the SSP is used in the TL models LYBIN or RAM, it is interpolated to every 0.08 m and smoothed prior to this. The MATLAB function ”smooth” (a moving average filter) is used. As the SSPs only

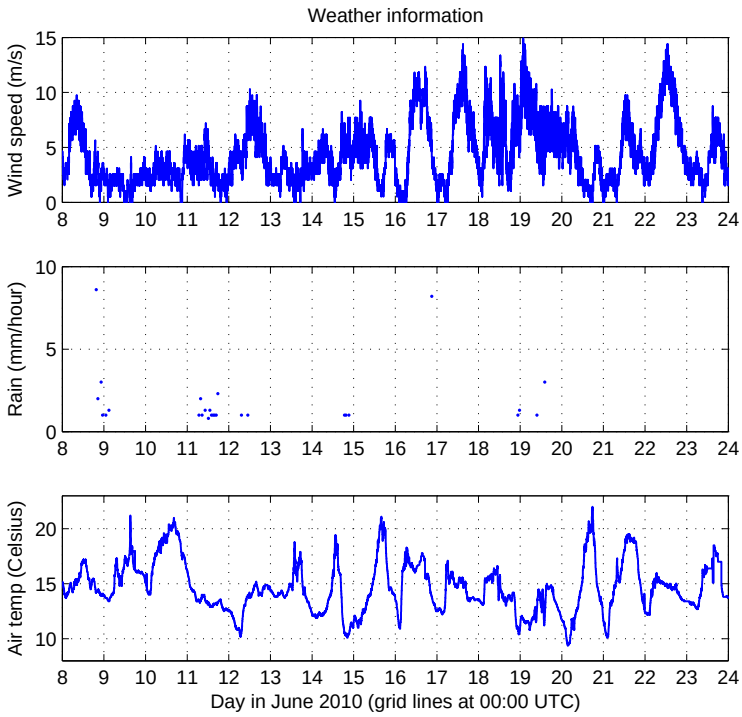

Figure 4.3: The plot shows the windspeed, rain and temperature for the relevant time period, measured by a weather station (Oregon Scientific WMR200) placed in the Inner Harbor of Horten. [17]

are measured down to about 100 m depth, the SSPs are extrapolated down to 200 m depth using the pressure effect. According to [13], one can use the simplification that the sound speed increases by 0.017 m/s pr meter for increasing depth (at 10 °C water temperature and normal environment conditions).

Bottom properties are found from a sea map from Kartverket, see Figure 4.1. In the map there is noted Cy, Cy M and S at some locations. This stands for a bottom composed of clay, clay and mud and sand, respectively. There is no other known survey of the bottom properties in this area. In [21], there are listed some typical values for geoacoustic properties connected to certain bottom types, and these can be seen in Table 4.2 for clay, silt and sand. At Breiangen, the seabed has some elevation where the bottom can be harder with rock characteristics, but this will not be taken into consideration.

The values in Table 4.2 for the relevant area of the ship passing will be used in RAM for TL estimation. LYBIN uses bottom types 1-9, where 1 is hard, and 9 is soft. In [22], the LYBIN bottom type number has been tested against different

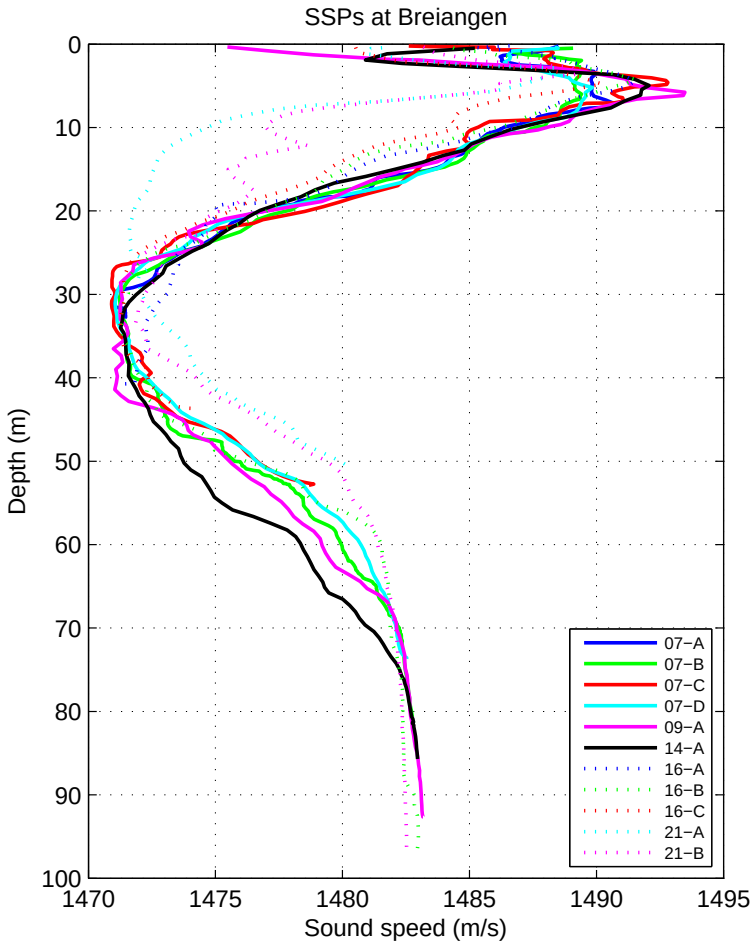

Figure 4.4: The plot shows the SSPs measured at Breiangen outside Horten in the month of June. The number in the legend indicates the date, and the letters indicate different locations. [17]

values for bottom parameters. The best fit for a bottom type number for clay, silt and sand in LYBIN is 4, 3 and 2 respectively, and can be seen in Table 4.2 under corresponding LYBIN bottom type number. There is no specific values for mud, but it should be somewhere between clay and silt.

Bottom profiles are delivered from FFI. The profiles have a range of about 3 km and start at the location of NILUS-C, and there is one profile for every 10 degrees in a circle pivoting NILUS-C. This means that the profiles probably will not match exactly the angle between the ship and the node, but will not be further off than 5 degrees. The profiles are discrete with a range step of 50 meters, but are inter-

Table 4.2: Geoacoustic properties for the bottom types clay, sand and silt. [21]

Bottom type	Density [kg/m^3]	Compressional wave speed [m/s]	Compressional wave attenuation [dB/λ]	Corresponding LYBIN bottom type number
Clay	1500	1500	0.2	4
Silt	1700	1575	1.0	3
Sand	1900	1650	0.8	2

polated to 1 meter and smoothed with the MATLAB function ”smooth” prior to be used in LYBIN and RAM. The depth in the bottom profiles for the relevant ship passings range between about 100 and 200 meters, with some variation, but will not be shown. The bottom profiles in connection with NILUS-D have not been available. But for the relevant passings, some bottom profiles from NILUS-C were a good match with regards to location and angles, and was thus used. This do however introduce some further uncertainty regarding the SL estimated from NILUS-D.

Chapter 5

Results

This chapter contains information about the ships that are analyzed and the resulting received level and estimated source level of the ships. The transmission loss for LYBIN, RAM and spherical spreading (denoted by r^2) connected to the source levels are also presented. All signal processing is done in MATLAB.

5.1 Ship information

In Table 5.1 the most relevant information about the ships is listed, such as the name, which NILUS-node was recording, ship-type, length, the accuracy of the GPS information, the speed at CPA, the distance at CPA, the average draft, the mean source depth and the standard deviation used in the distributed source model. In Table 5.2 the time at the start of each data window used for analysis together with the length of the window is shown. Note that the ships that did not experience amplitude clipping was at a range of about 800 m - 2000 m.

Table 5.1: A presentation of the analyzed ships and information about them.

Ship name	NILUS location	Ship-type	Length [m]	GPS accuracy	Speed [m/s]	Distance at CPA [m]	Draft [m]	Mean source depth [m]	σ [m]
Thebe	C	Cargo	89	High (<10 m)	5.9	765	3.9	2.2	0.5
Thebe	D	Cargo	89	High (<10 m)	5.9	1278	3.9	2.2	0.5
Autobank	C	Cargo	139	Low (>10 m)	10.4	483	6.5	3.7	0.8
Autobank	D	Cargo	139	Low (>10 m)	10.4	1564	6.5	3.7	0.8
Elektron II	C	Cargo	78	Low (>10 m)	5.8	540	3.5	2.0	0.4
Wilson Husum	C	Cargo	89	High (<10 m)	6.2	84	5.8	3.3	0.7
Wilson Husum	D	Cargo	89	High (<10 m)	6.2	2072	5.8	3.3	0.7

Table 5.2: Here the time at CPA for each ship is displayed, and the start and end of the data window period (DWP) used for analysis is shown for each ship. All the analyzed ship passings were at the 10th of June.

Ship name	NILUS location	Time at CPA	Length of DWP	Start of DWP centered at CPA	Start of DWP before CPA	Start of DWP after CPA	Start of DWP for noise	Length of noise DWP
Thebe	C	12:09:26	17 s	12:09:17	-	-	13:04:16	60 s
Thebe	D	12:08:36	16 s	12:08:28	-	-	12:17:21	60 s
Autobank	C	21:16:44	13 s	-	21:13:49	21:21:16	21:36:00	60 s
Autobank	D	21:16:29	13 s	21:16:22	-	-	16:11:14	30 s
Elektron II	C	10:09:15	17 s	-	10:06:36	10:10:41	11:36:20	30 s
Wilson Husum	D	19:43:29	16 s	19:43:21	-	-	14:12:38	30 s
Wilson Husum	C	19:44:48	16 s	-	19:41:16	19:44:39	19:20:14	30 s

5.2 Received level

The signal analysis described in section 2.1 is applied to the relevant ship passings. The received level (SPL) in dB re $1\mu\text{Pa}^2/\text{Hz}$ is estimated as a power spectrum density according to Eq. (2.13) for a spectrum of 1 Hz bands, and according to Eq. (2.16) for 1/3 octave bands. All levels are calculated with 50% overlap for each 1 s block of data (9000 samples) which are applied with a Hanning window of the same size. A 9000 point Fast Fourier transform is used which yields a Δf=1 Hz, or would otherwise have been normalized according to Eq. (2.9). Broadband levels are calculated as in Eq. (2.17) from 20 Hz to 1 kHz.

The spectrograms are calculated as a short-time Fourier transform with a Hanning window of size 16384 samples, a step size of 8192 samples (i.e. a 50% overlap), and adjusted to give the received level as a power spectrum density. This yields a $\Delta f \approx$0.5 Hz, and the levels are normalized to 1 Hz band levels.

Two ship passings (Thebe and Autobank) are chosen as examples of the received level analysis with main regards to background noise. A similar analysis has been done for the other ship passings, but these results are not in the main interest of this thesis and can be found in Appendix C. Noise adjustments are made to all ships, except Autobank at both locations and Wilson Husum at NILUS-C. However, in the remaining chapters, all levels will be described as noise adjusted, even if the SNR was adequate. Broadband received levels for each of the ships can be seen in Table 5.3 in section 5.4.

5.2.1 Thebe at NILUS-C

A spectrogram showing the RL of Thebe passing NILUS-C as frequency vs time can be seen in Figure 5.1. This is a good measurement with no visible interference from other ships, and the noise from the acoustic modem is not present at the CPA.

The received level as pressure vs. frequency for the passing of Thebe at CPA recorded by NILUS-C can be seen in Figure 5.2 for 1 Hz bands (left) and for 1/3 octave bands (right). The analysis time, or data window period, was 17 s, according to A.3. The broadband RL is 117.2 dB re $1\mu\text{Pa}^2$.

The background noise connected to Thebe and NILUS-C is chosen as a one minute period of low sound intensity about 55 minutes after CPA. It is estimated as a received level. The received level for the background noise as pressure vs. frequency is plotted in Figure 5.3 for 1 Hz bands (left) and for 1/3 octave bands (right). The broadband RL of the background noise is 93.9 dB re $1\mu\text{Pa}^2$.

The SNR is the RL of Thebe minus the RL of the background noise. The SNR vs frequency for the passing of Thebe at CPA is plotted in Figure 5.4 for 1 Hz bands (left) and for 1/3 octave bands (right). For frequencies where the SNR is less than

required, the RL is adjusted. The adjusted RL vs frequency for Thebe at CPA is plotted in Figure 5.5 for 1 Hz bands (left) and for 1/3 octave bands (right).

The difference in the noise adjusted RL vs the unadjusted RL vs frequency can be seen in Figure 5.6 for 1 Hz bands (left) and for 1/3 octave bands (right). The differences are very small, as a result of a high SNR, except for low frequencies. For 1 Hz bands the largest difference is about -2 dB, and in 1/3 octave bands the difference in the 10 Hz band is about -1 dB, in the 20 Hz band about -0.5 dB, and zero for all other bands.

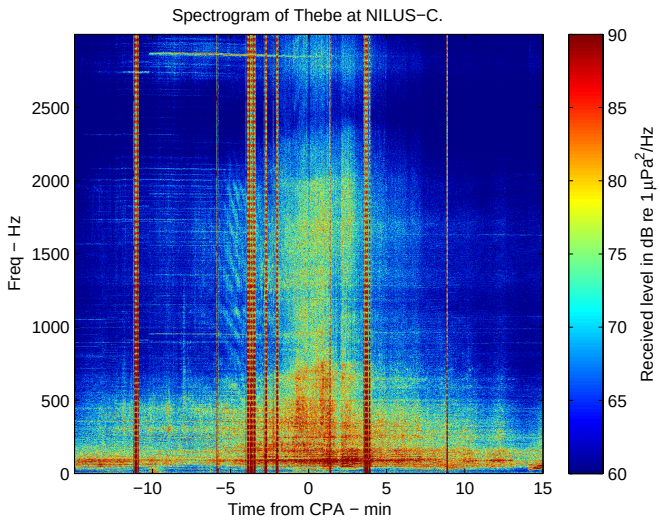

Figure 5.1: Spectrogram of Thebe at NILUS-C.

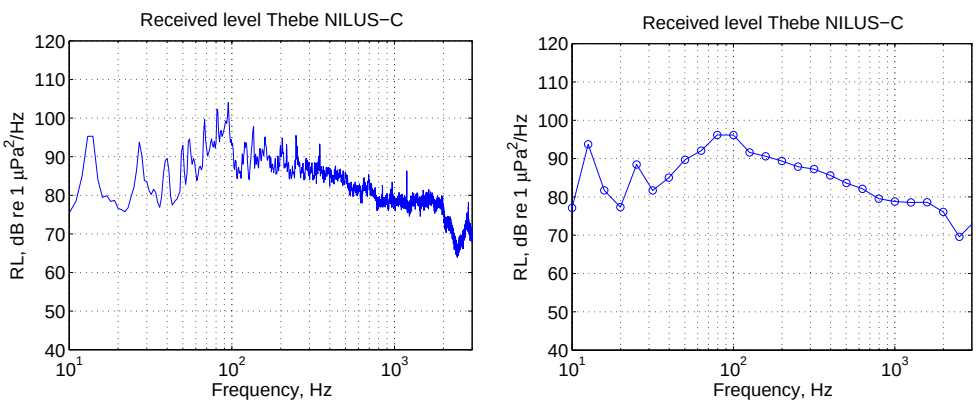

Figure 5.2: Received level vs frequency of Thebe at NILUS-C in 1 Hz bands (left) and in 1/3 octave bands (right).

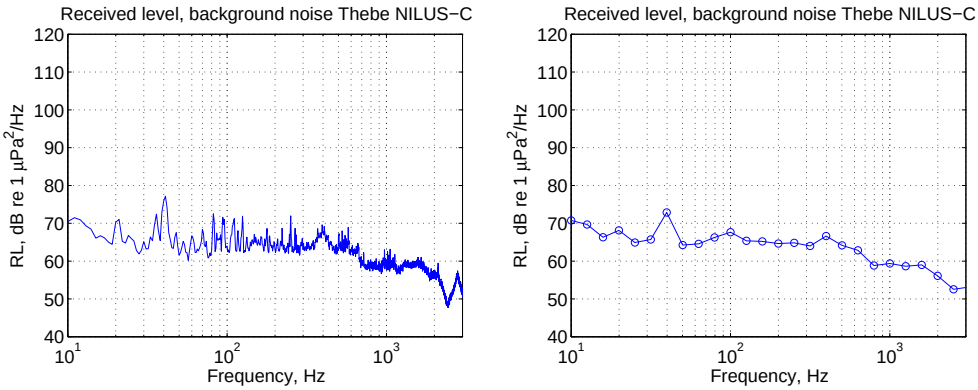

Figure 5.3: Received level vs frequency for the background noise of Thebe at NILUS-C in 1 Hz bands (left) and in 1/3 octave bands (right).

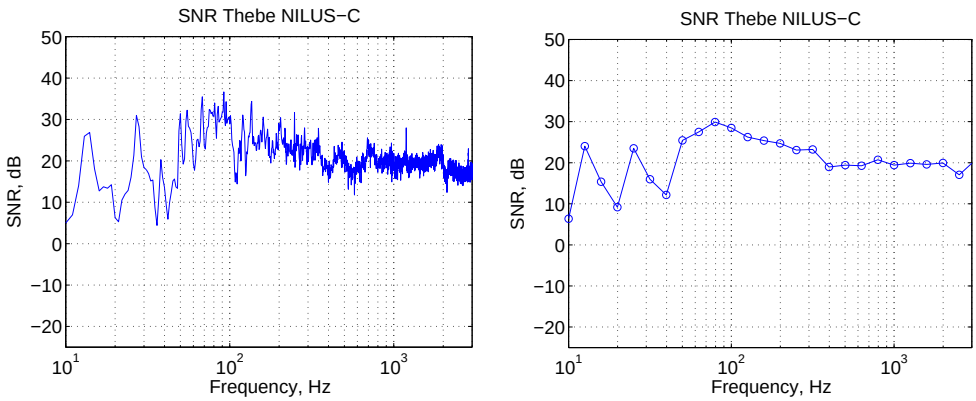

Figure 5.4: The SNR vs frequency for Thebe at NILUS-C in 1 Hz bands (left) and in 1/3 octave bands (right).

5.2.2 Autobank at NILUS-C

Because of the amplitude clipping of the recording near CPA, the measured RL and SL is taken as the average of a measurement before and after the visible clipping, each with a measurement time according to the DWP (13 s). The CPA of Autobank at NILUS-C was 483 m. The measurement of the ship before CPA was 2:48 minutes prior the CPA, and at a horizontal distance of 1820 m from the node. The measurement after CPA was 4:39 minutes after CPA, at a horizontal distance of 2959 m from the node. This yields an aspect angle of 15.4 degrees (re bow) before CPA, and 170.6 degrees (re bow) after CPA.

A spectrogram showing the RL of Autobank passing NILUS-C as frequency vs time can be seen in Figure 5.7. From the spectrogram it is clear that it is a good

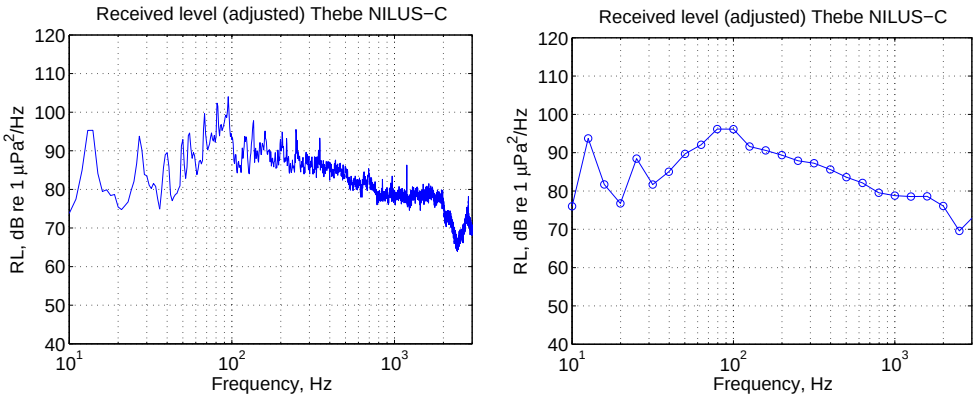

Figure 5.5: Adjusted received level vs frequency of Thebe at NILUS-C in 1 Hz bands (left) and in 1/3 octave bands (right).

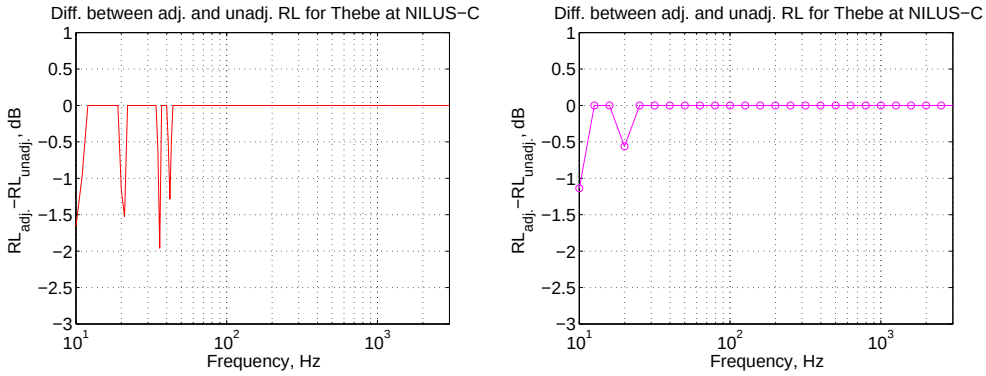

Figure 5.6: Difference between noise adjusted RL and unadjusted RL vs frequency of Thebe at NILUS-C in 1 Hz bands (left) and in 1/3 octave bands (right).

measurement with little interference from other ships, as the shape of the high intensity region of the received only indicates one present ship. One can also see that there is more noise after CPA, suggesting some angular (azimuthal) directivity towards the stern of the ships beam-pattern or it may be the result of propagation effects.

The received level vs frequency before and after CPA is plotted in Figure 5.8 for 1 Hz bands (left) and for 1/3 octave bands (right). The RL is slightly different before and after CPA, which can be expected due to the general angular directivity of ship noise [10]. The RL after CPA is a little higher than before CPA, even though it is over 1 km further away. The broadband RL before CPA is 126.5 dB re $1\mu\text{Pa}^2$, and 130.9 dB re $1\mu\text{Pa}^2$ after CPA.

The averaged RL vs frequency for Autobank is plotted in Figure 5.9 for 1 Hz bands (left) and for 1/3 octave bands (right). The average broadband RL is 128.0 dB re $1\mu\text{Pa}^2$.

The background noise connected to Autobank and NILUS-C is chosen as a 30 seconds period of low sound intensity about 18 minutes after CPA. The received level for the background noise as pressure vs. frequency is plotted in Figure 5.10 for 1 Hz bands (left) and for 1/3 octave bands (right). The broadband RL of the background noise is 92.5 dB re $1\mu\text{Pa}^2$.

The SNR vs frequency (the RL is the average of the RL before and after CPA) for the passing of Autobank is plotted in Figure 5.11 for 1 Hz bands (left) and for 1/3 octave bands (right).

As the SNR is within the requirements for the relevant frequencies, no adjustments are required. The SNR was high in this case as there was very little traffic in the surrounding time period, and because the ship passed at a relatively short range at high speed (10.4 m/s).

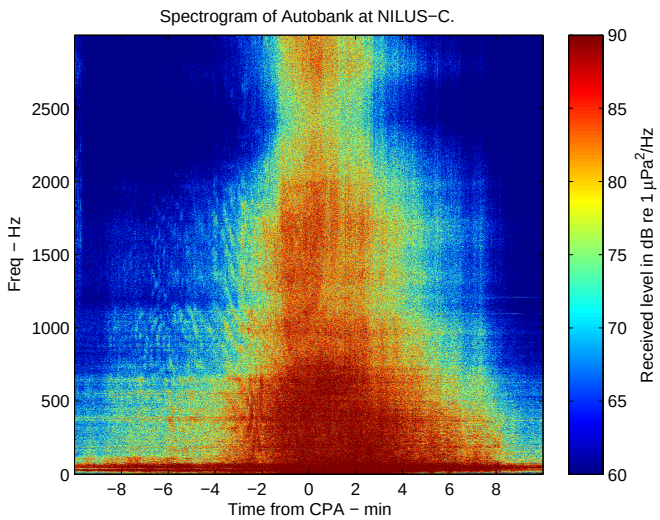

Figure 5.7: Spectrogram of Autobank at NILUS-C.

5.3 Source level and transmission loss

The main results from a ship noise measurement is the estimate of the monopole source level, as defined in section 3.1. To get the source levels, the same method as for the received level is used, but in addition TL is added. As can be seen in the SL algorithm flowchart in Figure 3.2, each of the 1 s long segments are applied with the TL for the range at that instant. The resulting source level is a power

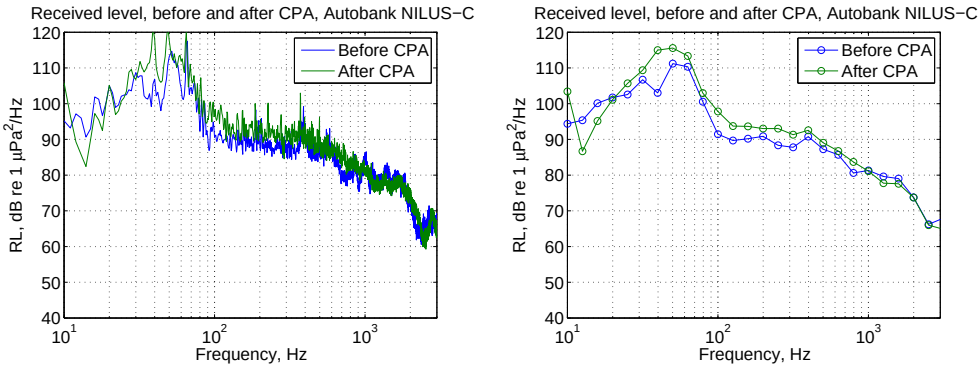

Figure 5.8: Received level vs frequency of Autobank before and after CPA at NILUS-C in 1 Hz bands (left) and in 1/3 octave bands (right).

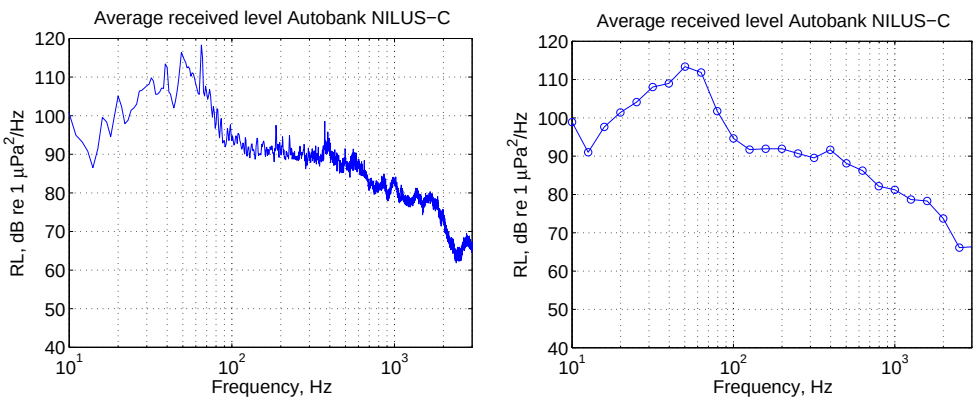

Figure 5.9: Averaged received level vs frequency of Autobank at NILUS-C in 1/3 octave bands.

spectrum density in dB re $1\mu\text{Pa}^2/\text{Hz}$ at 1 m, both i 1 Hz bands and 1/3 octave bands, in accordance with section 2.1. Broadband levels are calculated as in Eq. (2.17) from 20 Hz to 1 kHz. Broadband source levels for each of the ships can be seen in Table 5.3 in section 5.4.

For LYBIN and RAM, one bottom profile is used for each ship passing, except when the SL is estimated as an average of the SL before and after CPA; then an individual profile is used for each respectively. For all passings a bottom type of clay is assumed. No wind is used in LYBIN to make results from LYBIN and RAM more comparable. This is a reasonable simplification for a measured wind speed of about 4 m/s, as this has little impact on TL for ranges up to a few kilometers [1].

In LYBIN, the source depth is set as the effective source depth (ref. Eq. (3.1)), and in RAM the vertically distributed source model is applied (ref. Eq. (3.5)).

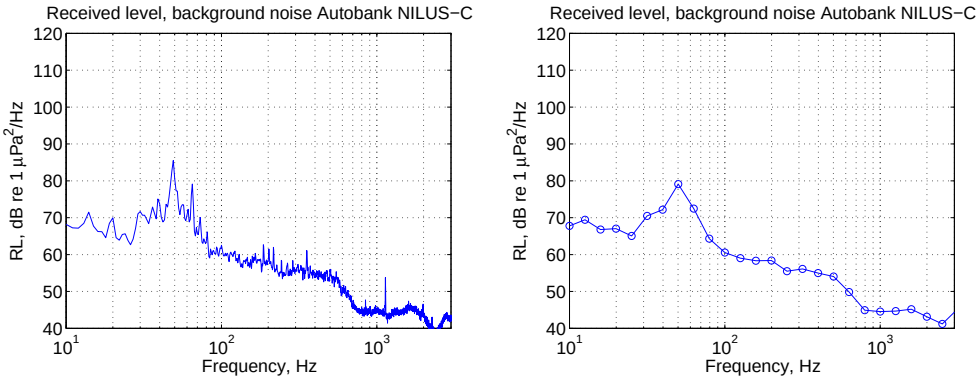

Figure 5.10: Received level vs frequency for the background noise of Autobank at NILUS-C in 1 Hz bands (left) and in 1/3 octave bands (right).

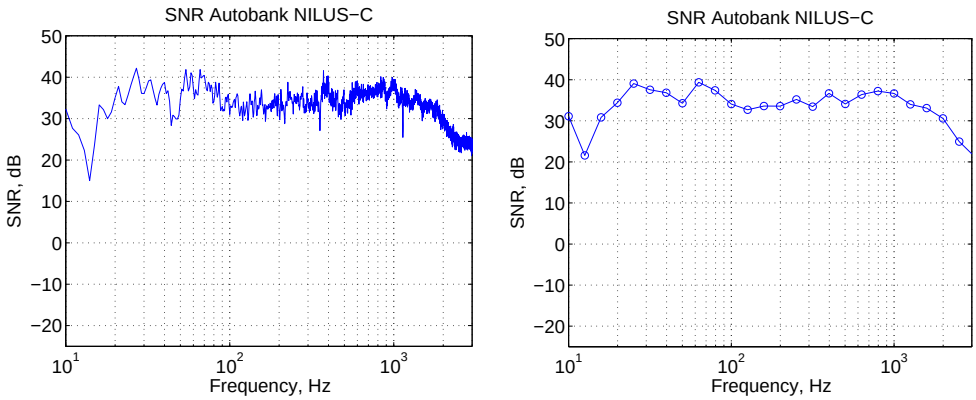

Figure 5.11: The SNR vs frequency for Autobank at NILUS-C in 1 Hz bands (left) and in 1/3 octave bands (right).

The depth discretization used in the source model is 0.15 meter. In LYBIN the TL is estimated for every 30 Hz, starting at 10 Hz and then interpolated to 1 Hz. In RAM the TL is estimated for every 5 Hz up to 50 Hz, then for every 10 Hz up to 100 Hz, then for every 20 Hz up to 320, then for the rest of the range for every 30 Hz, and then interpolated to 1 Hz. The TL from RAM at a specific range is averaged over ±10 meters, as the location of the receiver has an uncertainty of ±10 meters.

With the distributed source model, RAM has shown to give unstable TL levels for the combination of shallow source depths and low frequencies, e.g. less than 1.5 m and lower than 100 Hz for the current configurations. To prevent the low frequency part of the TLs to be corrupted, the unstable results from RAM is not included in the weighting process, and the normalization constant has been

changed to account for this. This will not change the result from the distributed source model significantly, as the low frequency part is mostly unaffected by the weighting. Section 5.3.1 shows an example of the analytical TL with a surface reflection (Figure 5.13) for a point source and a distributed source, and the low frequency part of those two are almost identical.

In the following sections the source level will be presented in 1 Hz bands and in 1/3 octave bands with a TL from RAM, LYBIN and spherical spreading for each measured ship. In addition, the TL for each of the models will be shown. This TL is the average of the TLs used for each segment in the data window.

Before the source levels are presented, an example of a TL from RAM with and without a distributed source model will be shown. Here also the TL from LYBIN and analytical Lloyd's mirror is shown.

5.3.1 Example of transmission loss results

To illustrate the effect of the vertically distributed source model applied to the TL from RAM, the TL for Thebe at NILUS-D with and without the model is presented. The TL vs frequency and range from RAM is shown in Figure 5.12, with an effective source depth of 2.2 meters (left) and a distributed source model (right). The TL vs frequency and range from an analytical expression is seen in Figure 5.13 with a point source (left) and a distributed source model (right), where the Lloyd's mirror effect is visible (a point source model is described in section B).

The ship was passing at a range of 1278 m. By comparing these two figures one can see that the Lloyd's mirror effect only is present in the TL from RAM up to about 500 m. This is also the case for the TL of Autobank at NILUS-C and D and Wilson Husum at NILUS-D (plots are not shown), but the range to the transition varies. This is mostly due to refraction and some bottom interaction creating a more diffuse field for longer ranges. For the passings of Thebe, Elektron II and Wilson Husum at NILUS-C, the Lloyd's mirror effect is present for the whole range, but because of the distributed source model, the loss in the low intensity region is only about 5 dB different. For the lowest frequencies the TL is still very high due to the Lloyd's mirror effect for the whole range. Still, for longer ranges and higher frequencies, the TL with a distributed source model is less varying than for a point source.

In Figure 5.14 the TL vs frequency and range is plotted for spherical spreading (left) and LYBIN (right). One can see that LYBINs TL is not very frequency dependent, and resembles spherical spreading without the LM effect.

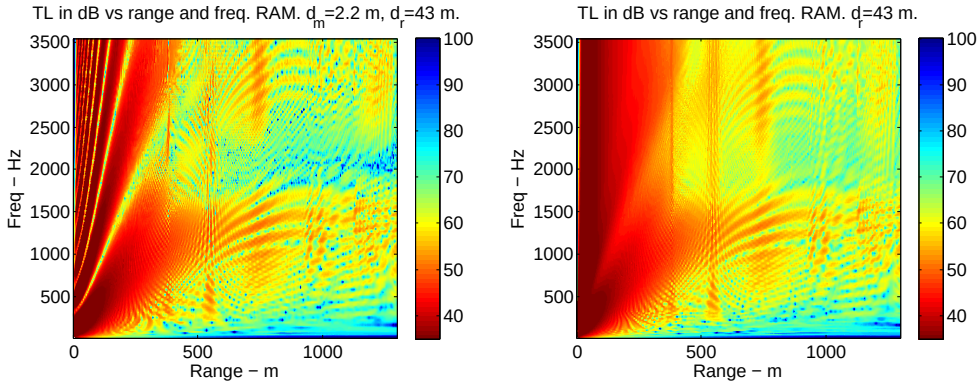

Figure 5.12: TL vs frequency and range from RAM for the ship Thebe passing NILUS-D, with a point source (left) and a distributed source (right).

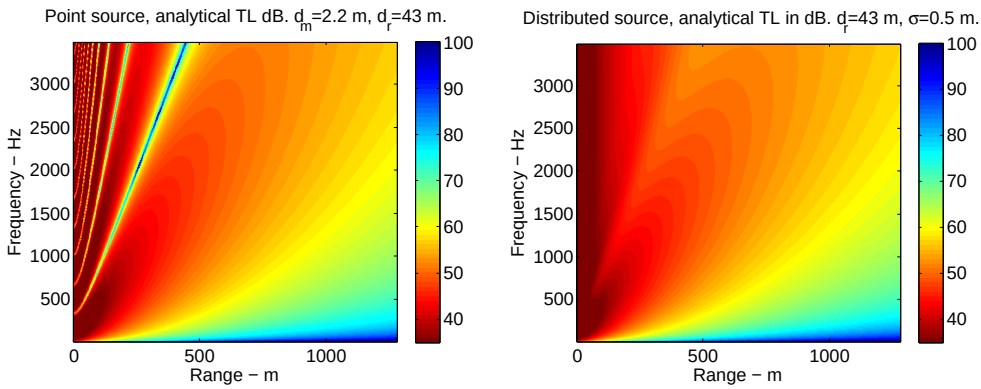

Figure 5.13: TL vs frequency and range from an analytical expression for spherical spreading including surface reflection (Lloyd's mirror effect) for the ship Thebe passing NILUS-D, with a point source (left) and a distributed source (right).

5.3.2 Source level and transmission loss estimates

First, the TLs and SLs of the ships that are measured at broadside are introduced. For Thebe at NILUS-C and D, Autobank and Wilson Husum at NILUS-D, the average TL from spherical spreading, RAM and LYBIN used in the SL estimation is plotted in Figures 5.15, 5.16, 5.18 and 5.21 respectively, for 1 Hz bands (upper left) and for 1/3 octave bands (upper right). For the same ships, the estimated adjusted source level is plotted in Figures 5.15, 5.16, 5.18 and 5.21 respectively, for 1 Hz bands (lower left) and for 1/3 octave bands (lower right) with a TL from spherical spreading, RAM and LYBIN.

Secondly, the TLs and SLs of the ships that are measured before and after CPA is

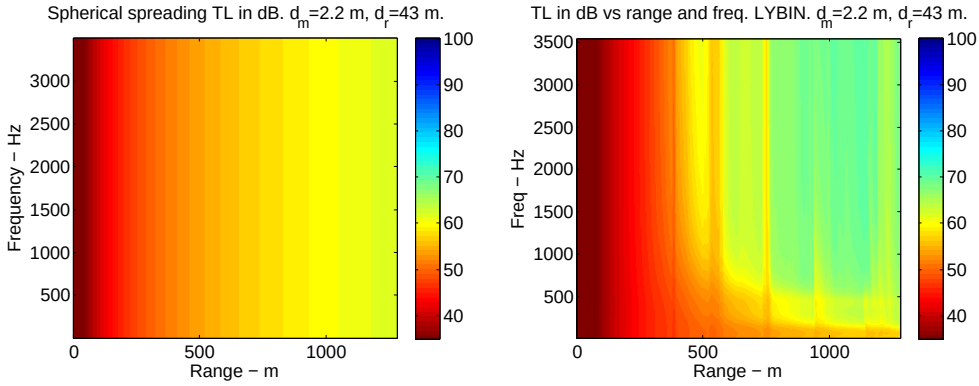

Figure 5.14: The plots shows the TL vs frequency and range for spherical spreading (left) and LYBIN (right), for the ship Thebe passing NILUS-D.

introduced. The TLs (from RAM) presented for these ships will in addition to the average TL of each SL, include the average TL of the measurement before CPA, and the average TL of the measurement after CPA. For Autobank, Elektron II and Wilson Husum at NILUS-C, the average TL from spherical spreading, RAM and LYBIN used in the SL estimation is plotted in Figures 5.17, 5.19 and 5.20 respectively, for 1 Hz bands (upper left) and for 1/3 octave bands (upper right). For the same ships, the estimated average adjusted source level is plotted in Figures 5.17, 5.19 and 5.20 respectively, for 1 Hz bands (lower left) and for 1/3 octave bands (lower right) with a TL from spherical spreading, RAM and LYBIN.

5.4 Summary of results

Here a summary of the results is presented.

5.4.1 Summary of source level estimates

The SLs in Figures 5.15, 5.16, 5.17 5.18, 5.19, 5.20 and 5.21 show a general tendency of agreement (less than 10 dB difference) for the different TL models for frequencies above 200 Hz - 300 Hz, with some exceptions. For lower frequencies the SLs with TL from RAM is generally 10 - 30 dB higher than the two others. The TL from LYBIN is about 5 dB lower than the TL from spherical spreading for frequencies below 100 Hz for all the measured ships.

The source level (RAM) for Autobank at NILUS-C is especially high.

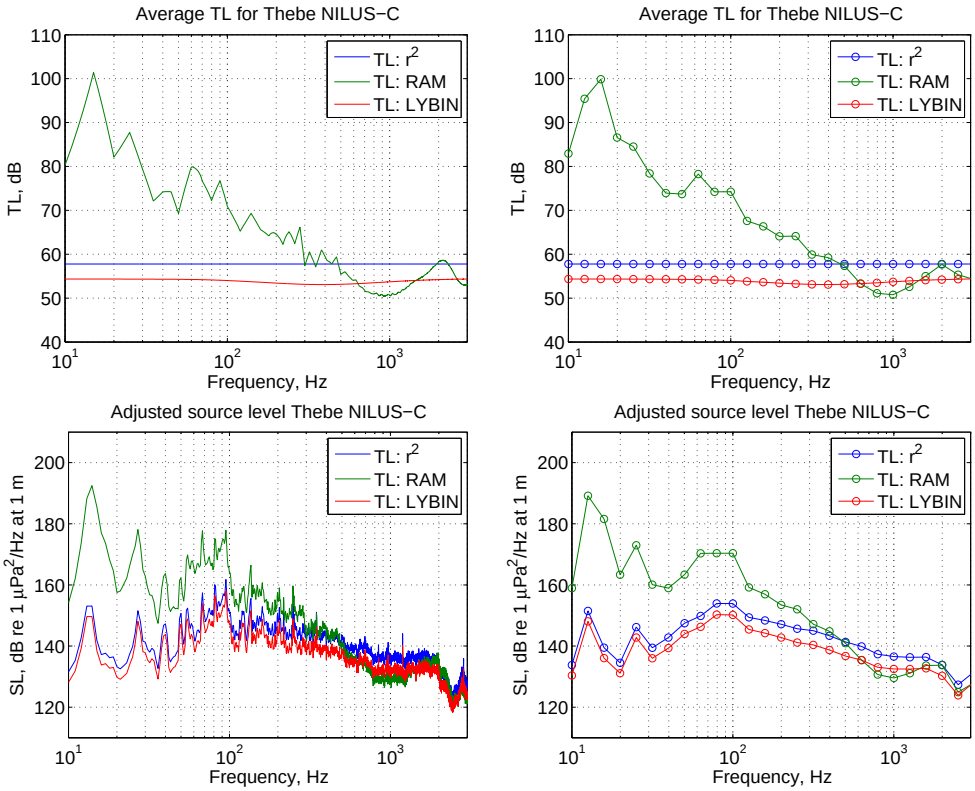

Figure 5.15: Upper sub-figures: Average transmission loss vs frequency of Thebe at NILUS-C in 1 Hz bands (left) and in 1/3 octave bands (right). The TL from spherical spreading, RAM and LYBIN is shown. Lower sub-figures: Adjusted source level vs frequency of Thebe at NILUS-C in 1 Hz bands (left) and in 1/3 octave bands (right). The SL is shown with three different TLs: Spherical spreading, RAM and LYBIN.

5.4.2 Broadband source levels

In Table 5.3, the broadband RL (20 Hz - 1 kHz) of the background noise and the ship is shown, together with the broadband SL (20 Hz - 1 kHz) for each of the TL models, according to Eq. (2.17).

From these values it is clear that the BSL with TL from RAM is considerably higher than the two others. For Thebe and Autobank the BSL (RAM) is about 12 dB higher at NILUS-C than at NILUS-D. With LYBIN the differences are smaller. For Wilson Husum the difference is larger for LYBIN than for RAM.

The broadband source levels vs speed with TL from RAM is plotted in Figure 5.22 for all the ships measured.

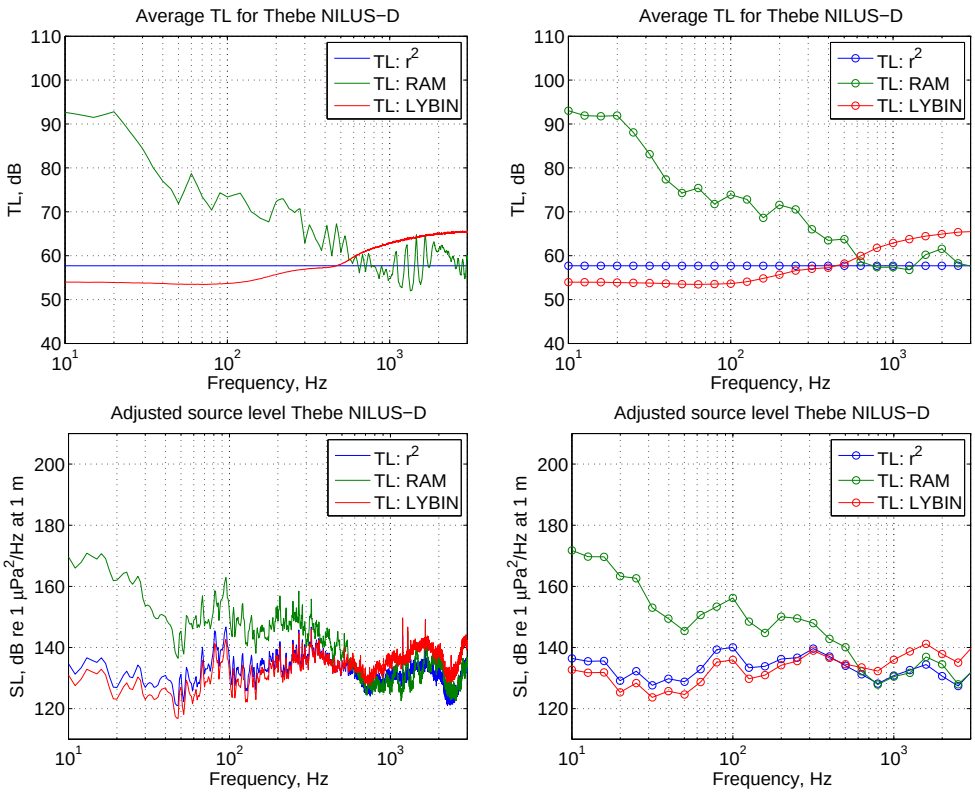

Figure 5.16: Upper sub-figures: Average transmission loss vs frequency of Thebe at NILUS-D in 1 Hz bands (left) and in 1/3 octave bands (right). The TL from spherical spreading, RAM and LYBIN is shown. Lower sub-figures: Adjusted source level vs frequency of Thebe at NILUS-D in 1 Hz bands (left) and in 1/3 octave bands (right). The SL is shown with three different TLs: Spherical spreading, RAM and LYBIN.

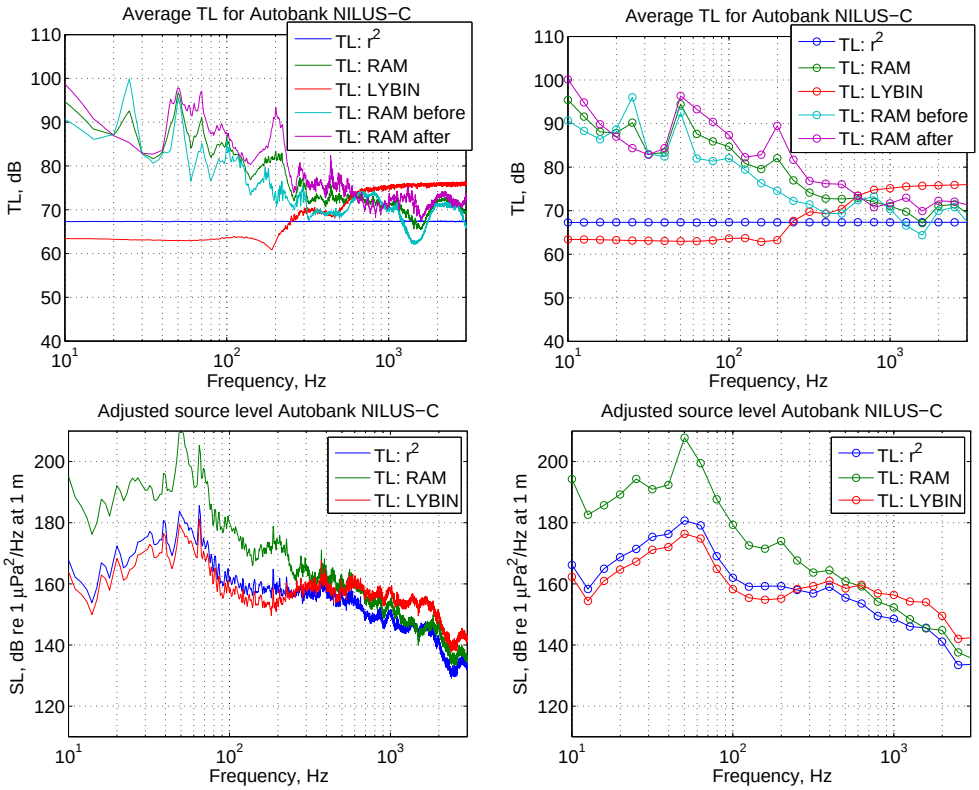

Figure 5.17: Upper sub-figures: Average transmission loss vs frequency of Autobank at NILUS-C in 1 Hz bands (left) and in 1/3 octave bands (right). The TL from spherical spreading, RAM and LYBIN is shown, including the TL from RAM before and after CPA. Lower sub-figures: Average adjusted source level vs frequency of Autobank at NILUS-C in 1 Hz bands (left) and in 1/3 octave bands (right). The SL is shown with three different TLs: Spherical spreading, RAM and LYBIN.

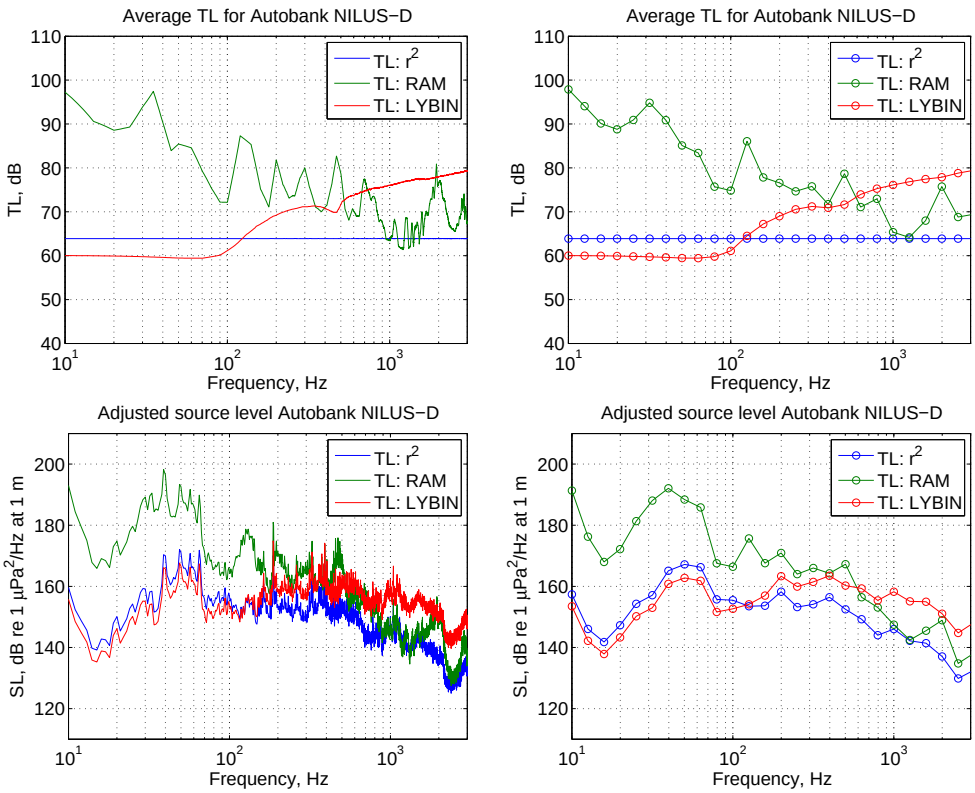

Figure 5.18: Upper sub-figures: Average transmission loss vs frequency of Autobank at NILUS-D in 1 Hz bands (left) and in 1/3 octave bands (right). The TL from spherical spreading, RAM and LYBIN is shown. Lower sub-figures: Adjusted source level vs frequency of Autobank at NILUS-D in 1 Hz bands (left) and in 1/3 octave bands (right). The SL is shown with three different TLs: Spherical spreading, RAM and LYBIN.

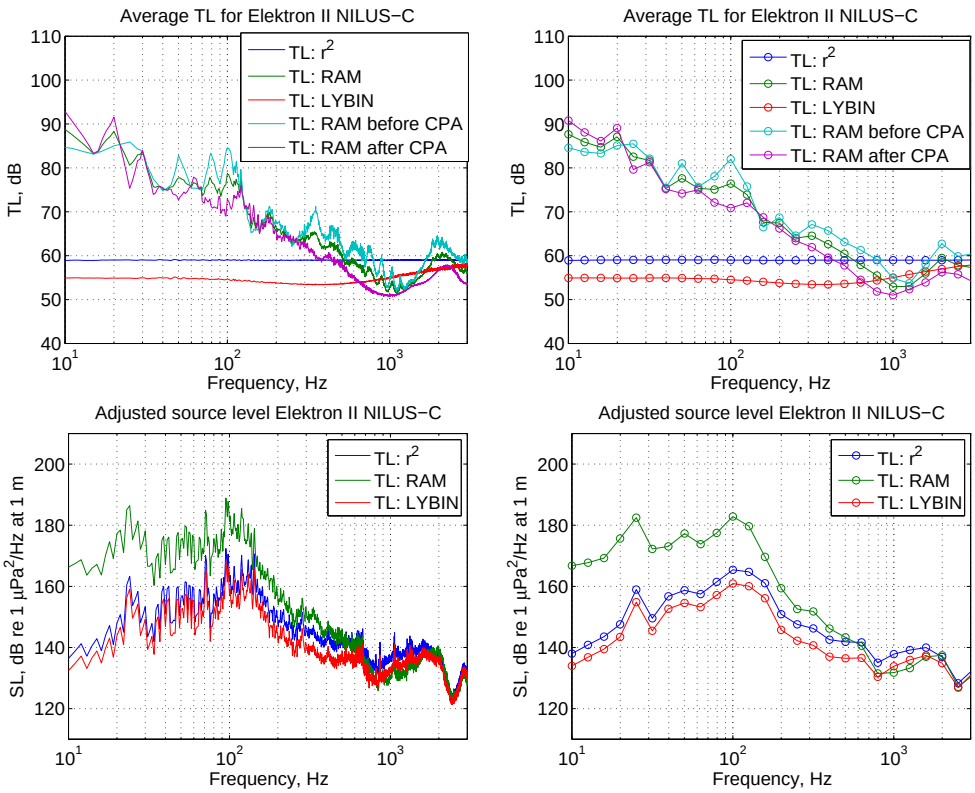

Figure 5.19: Upper sub-figures: Average transmission loss vs frequency of Elektron II at NILUS-C in 1 Hz bands (left) and in 1/3 octave bands (right). The TL from spherical spreading, RAM and LYBIN is shown, including the TL from RAM before and after CPA. Lower sub-figures: Average adjusted source level vs frequency of Elektron II at NILUS-C in 1 Hz bands (left) and in 1/3 octave bands (right). The SL is shown with three different TLs: Spherical spreading, RAM and LYBIN.

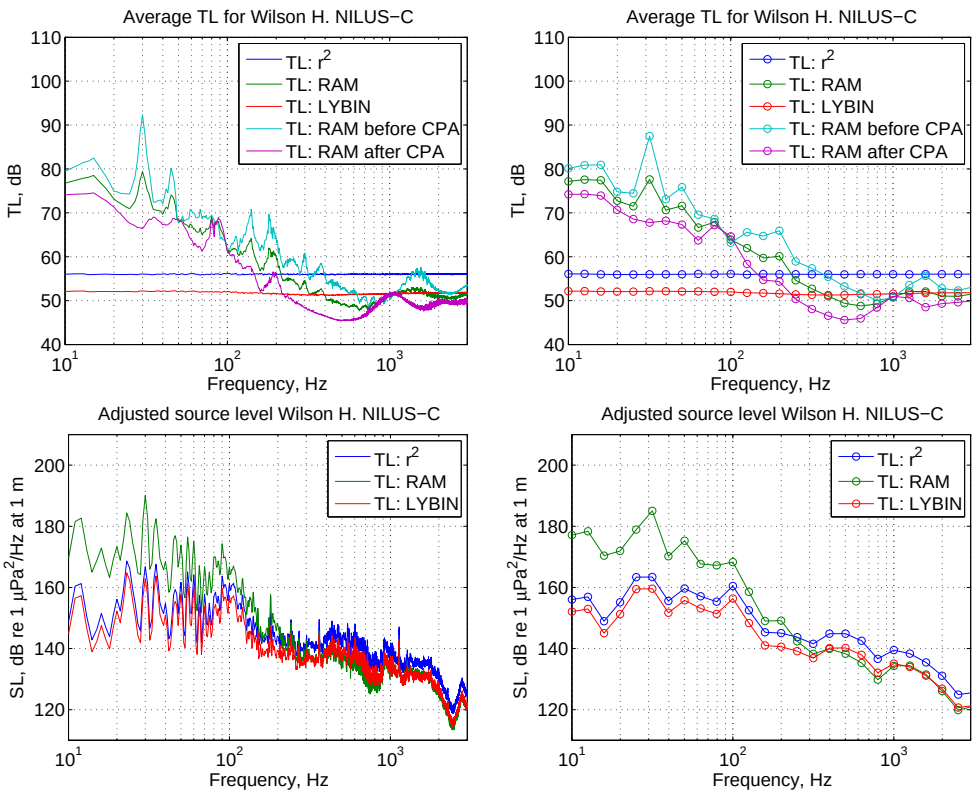

Figure 5.20: Upper sub-figures: Average transmission loss vs frequency of Wilson Husum at NILUS-C in 1 Hz bands (left) and in 1/3 octave bands (right). The TL from spherical spreading, RAM and LYBIN is shown, including the TL from RAM before and after CPA. Lower sub-figures: Average adjusted source level vs frequency of Wilson Husum at NILUS-C in 1 Hz bands (left) and in 1/3 octave bands (right). The SL is shown with three different TLs: Spherical spreading, RAM and LYBIN.

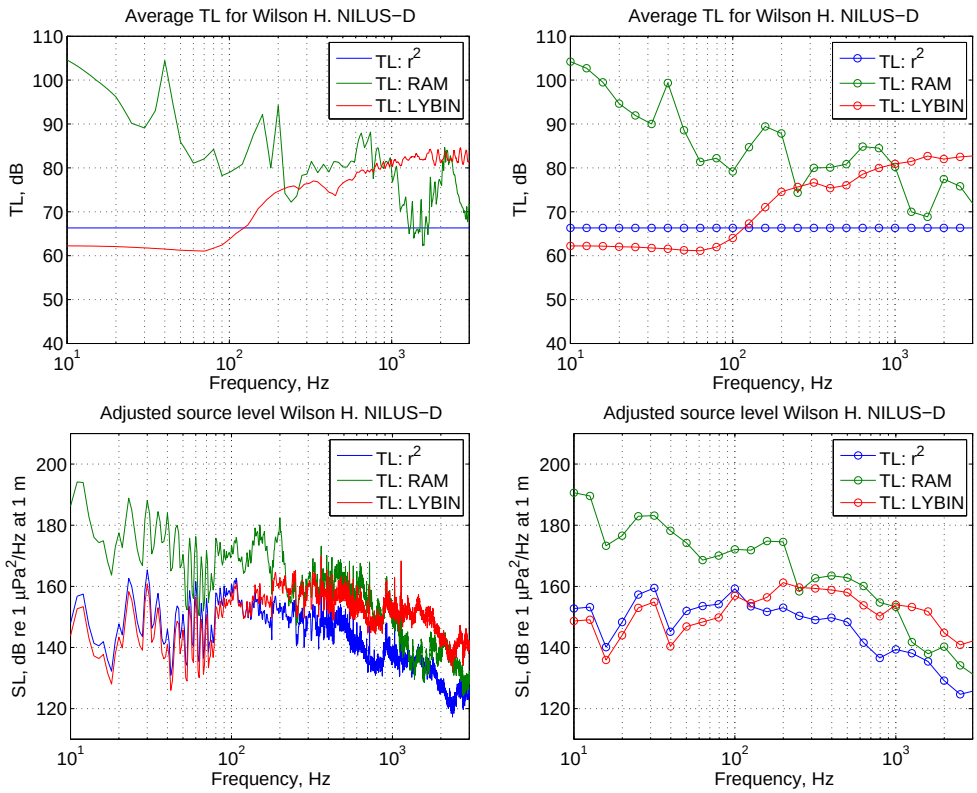

Figure 5.21: Upper sub-figures: Average transmission loss vs frequency of Wilson Husum at NILUS-D in 1 Hz bands (left) and in 1/3 octave bands (right). The TL from spherical spreading, RAM and LYBIN is shown. Lower sub-figures: Adjusted source level vs frequency of Wilson Husum at NILUS-D in 1 Hz bands (left) and in 1/3 octave bands (right). The SL is shown with three different TLs: Spherical spreading, RAM and LYBIN.

Table 5.3: A presentation of the analyzed ships broadband received level (BRL) and broadband source level (BSL). The broadband levels are calculated from the noise adjusted PSDs from 20 Hz to 1 kHz. For the ships that are not measured at the broadside, the broadband level is calculated from the average RL or SL of the levels before and after CPA.

Ship name	NILUS node	Broadside measure-ment	Backg. noise BRL [dB re $1\mu Pa^2$]	BRL [dB re $1\mu Pa^2$]	BSL (r^2) [dB re $1\mu Pa^2$ at 1 m]	BSL (RAM) [dB re $1\mu Pa^2$ at 1 m]	BSL (LYBIN) [dB re $1\mu Pa^2$ at 1 m]
Thebe	C	Yes	93.9	117.2	174.9	189.2	170.9
Thebe	D	Yes	94.8	107.0	164.8	177.4	164.7
Autobank	C	No	92.5	128.0	195.3	218.7	192.3
Autobank	D	Yes	84.8	121.3	185.2	205.7	189.6
Elektron II	C	No	105.2	125.1	184.1	199.7	179.5
Wilson Husum	C	No	101.6	123.8	179.8	194.4	175.7
Wilson Husum	D	Yes	96.7	113.3	179.7	199.0	186.5

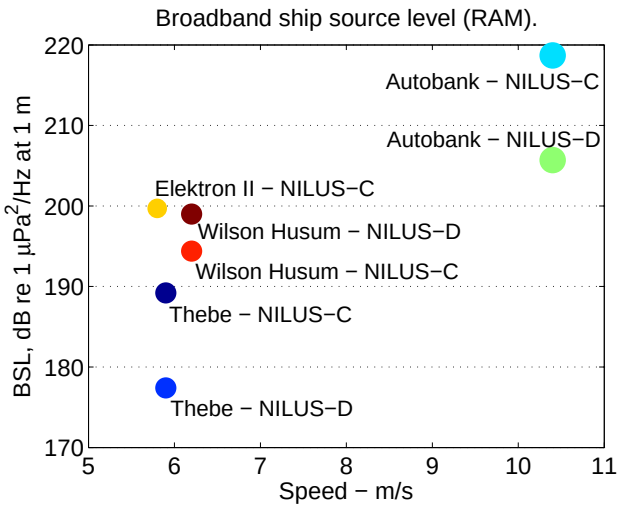

Figure 5.22: The broadband source level vs speed for each of the measured ships with a TL from RAM. The area of the circle illustrate the relative length of the ship.

5.4.3 1/3-octave band source levels at selected frequencies

In Table 5.4, the SLs for a representative selection of 1/3 octave bands for each of the ships and TL models are listed. The 1/3 octave band source levels are calculated according to Eq. (2.16).

5.4.4 Comparison of estimates from two sensors

Some of the passings were recorded at both NILUS-C and NILUS-D locations. It is interesting to see if the levels measured by both of them are comparable. A comparison of the SL vs frequency from NILUS-C and D for the ships Thebe, Autobank and Wilson Husum in 1 Hz bands is shown in Figures 5.23, 5.24 and 5.25 respectively, with TL from RAM (left) and TL from LYBIN (right). It would be better to use 1/3 octave bands to present this comparison, as the levels would be more stable. However, it is interesting to see if the distinct frequencies of the ships are present in both measurements, and if they are in accordance with each other. That is not possible to see in 1/3 octave bands.

The SL of Thebe and Autobank at both locations seems to be in reasonable agreement for higher frequencies than about 250 Hz for RAM, but somewhat less for LYBIN. For lower frequencies, SLs with LYBIN and RAM shows 5 dB - 15 dB higher levels at NILUS-C than at D. It is the opposite case for Wilson Husum, where the SL at NILUS-C and D agree well for frequencies below 100 Hz, and the

Table 5.4: The source levels in dB re $1\mu Pa^2/Hz$ at 1 m for the 1/3 octave bands 10 Hz, 31.5 Hz, 100 Hz, 315 Hz, 1 kHz and 3 kHz for all the ships and for each TL model.

Ship	Nilus location	TL model	1/3 octave band SL in dB re $1\mu Pa^2/Hz$ at 1 m					
			10 Hz	31.5 Hz	100 Hz	315 Hz	1 kHz	3 kHz
Thebe	C	r^2	166.2	175.4	162.0	156.9	148.5	133.7
		RAM	194.3	191.0	179.3	163.7	152.2	135.2
		LYBIN	162.3	171.1	158.3	159.3	156.4	142.4
Thebe	D	r^2	136.4	127.6	140.0	139.6	130.8	133.1
		RAM	171.8	153.0	156.2	148.0	130.5	132.9
		LYBIN	132.7	123.7	136.0	139.0	136.0	140.9
Elektron II	C	r^2	138.0	149.5	165.4	146.2	137.8	133.2
		RAM	166.7	172.2	182.8	151.8	131.8	131.3
		LYBIN	134.0	145.4	160.9	140.7	133.9	132.1
Autobank	C	r^2	166.2	175.4	162.0	156.9	148.5	133.7
		RAM	194.3	191.0	179.3	163.7	152.2	135.2
		LYBIN	162.3	171.1	158.3	159.3	156.4	142.4
Autobank	D	r^2	157.4	157.1	155.5	154.1	146.0	132.6
		RAM	191.3	188.1	166.4	166.0	147.5	138.2
		LYBIN	153.5	153.0	152.7	161.4	158.2	148.2
Wilson H.	C	r^2	156.0	163.4	160.5	141.5	139.5	125.6
		RAM	178.6	187.1	170.0	139.9	133.1	121.2
		LYBIN	152.1	159.6	156.4	136.9	135.1	121.4
Wilson H.	D	r^2	152.8	159.5	159.2	149.0	139.4	126.0
		RAM	192.1	185.1	174.2	163.5	153.7	131.1
		LYBIN	148.7	154.9	157.0	159.3	154.0	142.5

SL from NILUS-D is higher by up to 25 dB for higher frequencies, for both RAM and LYBIN. For Thebe, distinctive frequencies which compose a ships acoustic signature can be seen from both NILUS-C and D in the frequency range 40 Hz to about 100 Hz. For Wilson Husum these frequencies matches remarkably well down to 10 Hz.

5.5 Uncertainty

There are several factors that contribute to uncertainties in the SL estimate. Here these factors will be described.

One of the main uncertainties arises from the acoustic sensor on the NILUS-node. In the specification, [19], the sensitivity of the element has an accuracy of ±3.0 dB. This represents the maximum deviation from nominal hydrophone sensitivity for a large production series of hydrophones. In practice, an accuracy of <1.0 dB can be

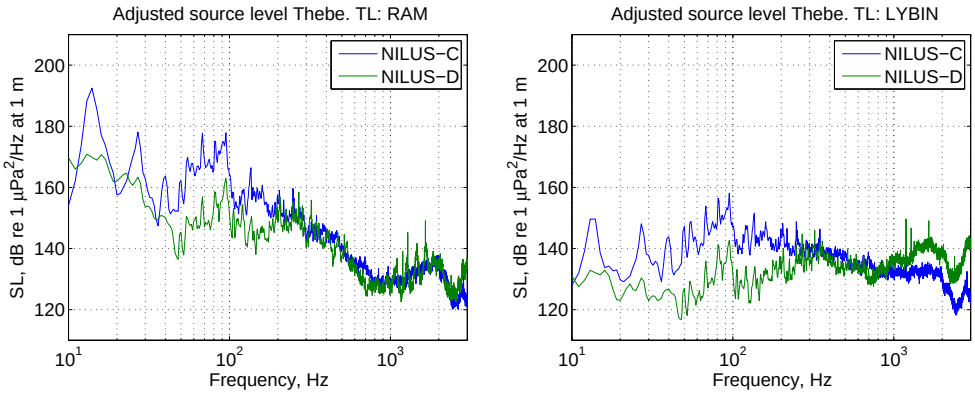

Figure 5.23: The SL vs frequency of Thebe in 1 Hz bands measured at NILUS-C and D, with TL from RAM (left) and TL from LYBIN (right).

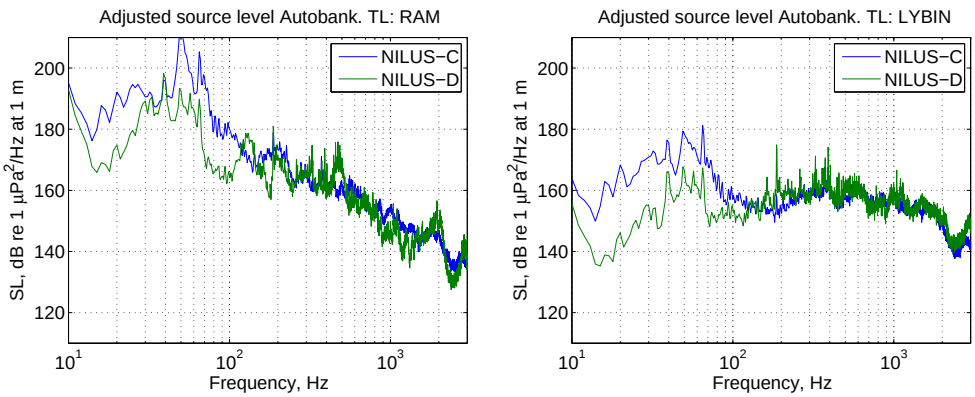

Figure 5.24: The SL vs frequency of Autobank in 1 Hz bands measured at NILUS-C and D, with TL from RAM (left) and TL from LYBIN (right).

assumed. However, in the following discussion, and since a dedicated calibration measurement for the NILUS nodes was not available, the factory specification of 3 dB will be used. This uncertainty will be in the SL independently of which TL model is used.

The signal processing introduces some uncertainty. The ANSI standard gives ±0.5 dB as a typical value for the data processing uncertainty [7].

The received level will thus have an combined uncertainty from the sensitivity and signal processing by taking the root of the sum of the squares (RSS), that is ±3.0 dB.

The received levels for all the ships (including background noise measurements) experience a reduction of up to 10 dB at around 2 kHz to 2.5 kHz. Since it

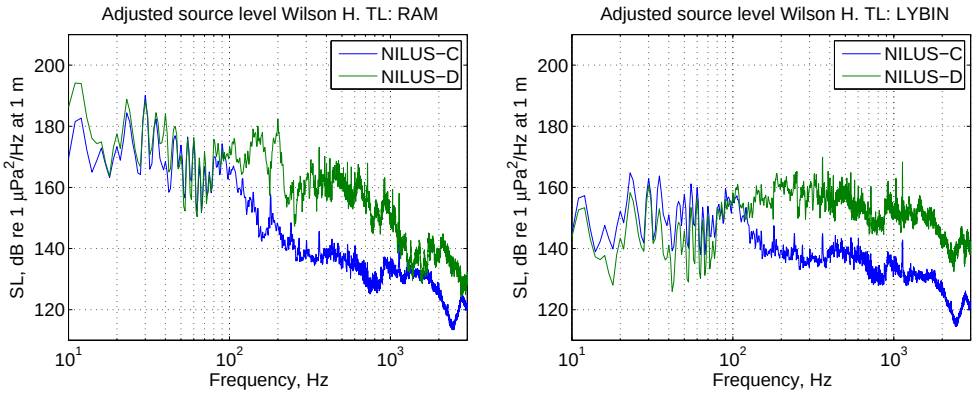

Figure 5.25: The SL vs frequency of Wilson Husum in 1 Hz bands measured at NILUS-C and D, with TL from RAM (left) and TL from LYBIN (right).

is seen regardless of what is measured, it may be a property of the acquisition system, where one possibility is that the acoustic sensor has an unwanted frequency response in that frequency range. Another possibility is that the geometrical shape and material of the tripod unit the sensor is mounted on, combine to dampen certain frequencies. As such, the results at frequencies above 2 kHz should be viewed with this in mind.

The AIS data indicates a location accuracy that is either higher or lower than 10 meters. The AIS documentation [11] does not specify any more than that. As the default reporting value for the GPS accuracy is higher than 10 m, the GPS accuracy is probably better in many cases, as it may not have been set in the AIS transmitter. Regardless, a location accuracy of 10 m will be assumed for all the GPS data from the AIS. The NILUS-node has a location accuracy of about 10 m [17].

The GPS antenna position on the ship may also contribute to a bias in the measured range. However, all the ships antennas was placed within 2 meters of the center (port-starboard direction) of the ships. The antenna position has been used as the ships acoustic center (bow-stern direction), which is only 8 m, 15 m and 9 m from the stern of the ships Thebe, Elektron II and Wilson Husum respectively, and is a reasonable approximation to the suggested acoustic center described in the standard. For Autobank however, the antenna location is 116 m from the stern of the ship. This distance in bow-stern direction has little impact on the range, and is within the 10 m accuracy of the positioning system. But it does affect the timing of the data window, which will now be placed about 10 s too early compared to a propeller-based acoustic center. However, at the current ranges the angle between CPA and the ship changes slowly, and it will still be a broadside measurement.

For the measurements at NILUS-D, the bottom profiles used are taken from bottom

profiles originating from NILUS-C, which deviate in a small degree from the real environment in the relevant situations. This introduces some uncertainty regarding the results from NILUS-D.

The drafts used in the measurements are average values of the reported drafts. The reported drafts varied by about 1 meter for some of the cases. As the source depths used in the models are based on the drafts, a typical uncertainty for the source depth could be ±1 meter. This mostly affects the SL with TL from RAM, as a small change in source depth has an insignificant impact on the TL from LYBIN and spherical spreading. The receiver depth has an uncertainty of about ±3 meters, but that is not significant with regards to its impact on TL (incoherently).

Table 5.5: Overview of how much different factors influence the TL in dB at the ranges 200 m, 700 m and 2000 m [1].

	Parameter	200 m range	700 m range	2000 m range	Coherent effect	Frequency dependent
1	Range, 10 m change	1.0	0.5	0.1	Yes	Yes
2	Source depth 1 m change	0.2	4	3	Yes	Yes
3	Rec. depth 5 m change	0.2	1.5	0.3	Yes	Yes
4	Bottom type 3 vs 4	0.1	0.4	0.8	No	No
5	Const. SSP vs real	0	0	3	No	Yes
6	Range 10 m change	0.4	0.1	0.04	No	No

In Table 5.5 an overview is given of how much different factors influence the TL when changed. These values were found in [1]. The influence is looked at for the ranges 200 m, 700 m and 2000 m. It has been looked at both coherent effects, where worst case values are given for a typical ship set-up, and also some cases in LYBIN where different bottom types and sound speed profiles are used. However, the values listed for coherent effects will change some for different source-depths and drafts. In addition, the change in TL for spherical spreading is shown when the range is decreased by 10 m. The change in TL for a bottom-type of 3 vs 4 in LYBIN can be realistic, as the bottom-type not necessary is exactly as specified by the map in Figure 4.1. The change in TL for a constant SSP vs a real SSP is also realistic, but should not be used in uncertainty estimation as the real profile is known and used.

As 700 m is the closest of the ranges most of the analyzed ships can be said to be measured at, one can try to combine the values in Table 5.5 for 700 m to give an estimate for the uncertainty of the transmission loss. It is not attempted to give an estimate for the uncertainty of each TL model, only a general estimate. The value for range is added twice, one time for the receiver and one time for the source. The combined RSS uncertainty at 700 m is then ±4.4 dB. Th RSS uncertainty for 200 m and 2000 m is ±1.6 dB and ±3.1 dB respectively.

The resulting SL uncertainty for the three ranges are then when including the RL uncertainty, ±3.4 dB ±5.3 dB and ±4.4 dB for 200 m, 700 m, and 2000 m, respec-

tively. The TL estimation clearly introduces an uncertainty in the SL as towards which of the transmission losses from RAM, LYBIN or spherical spreading is closest to the real TL. In summary, the most dominant uncertainty in the measurements comes from the uncalibrated hydrophone.

Chapter 6

Discussion

This thesis has developed a method for estimation of ship noise levels under non-ideal measurement conditions. The method is applied to acoustic data recorded at two sensor platforms deployed in the Oslofjord. The method extends ship noise source level estimation as specified in current measurement standards from controlled conditions typically only achieved in a dedicated measurement range to more general conditions of the shallow coastal ocean. Particular attention has been paid to the estimation of and correction for background noise level, the correction to monopole source level by use of acoustic propagation models including detailed construction of a model environment, and the use of auxiliary information for estimation of ship range.

There were some challenges in finding suitable ship passings in the analyzed data set. Due to difficult conditions at the measurement location because of heavy traffic, only a few ship passings were found to be usable for estimation of source levels. Amplitude clipping of ship passings with high intensity in several cases prevented use of short-range passings and led to measurements at longer distances than desirable. At longer distances the background noise and noise from other ships interfere with the measurement, and although background noise has been corrected for in the results in this thesis, this has led to ship passings being discarded from the data set.

The range measurement system used in the method is a key element in estimating the SL. This AIS based system enables the range to be estimated with high precision, relatively to the long range. Input to acoustic propagation models, such as an SSP, bottom profile and properties, source depth and wind, was included in the modeling of the measurement location. The same input was used for two such models, LYBIN and RAM. The frequency dependent transmission losses from RAM and LYBIN are quite different. They differ by up to 30 to 40 dB at the most for frequencies up to a few hundred hertz. For higher frequencies (above about 500 Hz) they are generally more in agreement. This may be explained by two things.

First, the high TL for low frequencies in RAM is caused mostly by the coherent Lloyd's mirror effect (see Figure 5.12 and 5.13). As LYBIN is incoherent, this effect is not seen (see Figure 5.14). Second, LYBIN is a high frequency approximation, and is for this reason in better agreement with RAM at higher frequencies.

The TL from RAM fluctuates rapidly with regards to range and frequency, as can be seen in Figure 5.12, which is mitigated by averaging over range as the receiver location has an uncertainty. LYBIN gives a TL that is less fluctuating with regards to range and frequency. As the TL from RAM is rapidly varying with frequency, one should be careful to use the resulting SL estimate in 1 Hz bands to determine the amplitude of signature frequencies. In general, because of the frequency variation of the TL, levels in 1/3 octave bands are more stable.

The source level for Autobank at NILUS-C is highest, with an estimated BSL (r^2) of 195.3 dB re $1\mu Pa^2$ at 1 m from one of the measurements. It is a large ship, and its speed is high, which may justify the high levels, in, e.g., [6], container ships of greater length and same speed has lower reported source levels. However, in the second measurements of this ship, the estimated BSL (r^2) is 185.2 dB re $1\mu Pa^2$ at 1 m which is in agreement with measurements of container ships in [6]. In the measurement standard, at least four measurement runs are required to give an average SL, resulting in a less variable SL. Unless measured by two NILUS-nodes simultaneously, this possibility is not available in this method. If the SL for Autobank is an average of the SL at NILUS-C and D, the BSL (r^2) would be 190.3 dB re $1\mu Pa^2$ at 1 m, which is more realistic. The average BSL (RAM) from the two locations is higher, 212.2 re $1\mu Pa^2$ at 1 m, however there are few other reported monopole SLs to compare against.

In most literature on ship source level estimation, the dipole source level is reported, e.g. [6], [10] and [23]. However some report monopole source levels estimated with a propagation loss model: [15] and [16]. The method in this thesis is particularly similar to the one used in [16], except in this thesis the TL is estimated for each individual ship passing for more frequencies, with a better description of the environment and with a distributed source model instead of a point source model.

The spectrograms of the RL of the ships does not reveal any clear influence of the Lloyd's mirror effect for the ships that should be influenced (not considering the lowest frequencies). However, it would only be within 5 dB, according to the distributed source model, and that is hardly noticeable. The parameters used in the distributed source model may not be the best fit for the ships. The model gives a better approximation to the assumed true source distribution than a point source model, however, in future work, improvements to the parameters such as a better estimate for the propeller diameter could result in a estimated TL that would match the real LM pattern even better. Based on the observation that Lloyd's mirror effect is diminished by refraction after a certain range, the incoherent model LYBIN may be relevant to use beyond this transition range, but low frequencies are still observed to be dominated by the LM effect.

Of the three methods used to correct for propagation effects in this thesis, two of them have shown to have certain restrictions. The spherical spreading model will be incorrect at longer ranges as both incoherent and coherent multipath effects are disregarded. LYBIN handles incoherent multipath effects, but not the dipole effect, and for long range and low frequencies underestimates the TL. Since RAM is coherent, multipath effects are handled correctly for all frequencies, and has thus been shown to be the best choice for a propagation model. In addition, the distributed source model should be used with RAM.

A reference measurement of the ships source level would be needed in order to consider the correctness of the method. This could be done in a measurement range, with a setting as described in the ANSI standard [7]. Alternatively, if measurements were made of a ship at close range, this could be used as a reference. This was, however, not possible with the current measurement equipment, due to the amplitude clipping at high levels.

Suggestions for improvements to the method, instrumentation and execution of the measurement are as follows.

- Resolve the amplitude clipping problem of the measurement equipment. This would allow measurement of ships at closer ranges or ships that have high source levels.
- Use the NILUS-nodes in locations where there is less traffic.
- Acquire source level estimates that could function as a reference. That would make it possible to evaluate the different TL models against each other.
- Find a better estimate of the source depth, draft and standard deviation in the distributed source model, as the current values are based on assumptions, and has a large impact on the resulting TL.

The most important contribution from the method and results presented in this thesis is that the RAM model with a distributed source model is the best choice for correcting to monopole source level estimates. This model can be used in unideal measurement locations but requires a detailed model description of the environment.

Chapter 7

Conclusion

A method for remote measurement of ship noise that applies the RAM acoustic propagation model with a distributed source model has been formulated and implemented. This method provides the monopole source level and is applicable to an unideal measurement location and geometry.

Estimates of the monopole source level of seven ships were produced and compared with dipole source level estimates. In general, it was found that only the RAM model can be used to produce monopole source level estimates. The close proximity of the sensor location to the shipping lane and the high sensitivity of the hydrophone prevented use of short-range data from loud ships, which would have been desirable for reference measurements. The high number of ships in the area also made several measurement periods unusable, as single ship data could not be isolated from background (ship) noise.

This method enables measurement of a ships monopole source level outside of the standard measurement context, and can help in the establishment of a general, easily deployable system for measurements of ship noise source levels in coastal regions.

Bibliography

[1] Stian Coward. *Method for remote sensing of acoustic ship noise.* Project thesis, Norwegian University of Science and Technology, 2012.

[2] Ellen Johanne Eidem and Knut A. Søstrand. Beregning av spektra og transmisjonstap ved hjelp av fft og filterbanker, June 2001, FFI (Norwegian Defence Research Establishment). FFI-rapport 2001/02101.

[3] John G. Proakis and Dimitris G. Manolakis. *Digital signal processing.* Pearson Prentice Hall, 4th edition, 2007.

[4] G. Heinzel, A. Rüdiger, and R. Schilling. Spectrum and spectral density estimation by the discrete fourier transform (DFT), including a comprehensive list of window functions and some new at-top windows. 2002.

[5] Steven W Smith. *The Scientist and Engineer's Guide to Digital Signal Processing*, volume 2. California Technical Publishing, 1997.

[6] Megan F. McKenna, Donald Ross, Sean M. Wiggins, and John A. Hildebrand. Underwater radiated noise from modern commercial ships. *The Journal of the Acoustical Society of America*, 131(1):92–103, 2012.

[7] Accredited Standards Committe S12 Noise. ANSI/ASA S12.64-2009/Part 1. Quantities and Procedures for Description and Measurement of Underwater Sound from Ships - Part 1: General Requirements. American National Standards Institute, Inc, 2009.

[8] Michael A. Ainslie. *Principles of Sonar Performance Modeling.* Springer, Chichester, UK, 2010.

[9] Michael D. Collins. User's guide for RAM versions 1.0 and 1.0p.

[10] Mark V. Trevorrow, Boris Vasiliev, and Svein Vagle. Directionality and maneuvering effects on a surface ship underwater acoustic signature. *Acoustical Society of America*, 124(2):767–778, 2008.

[11] International Telecommunications Union. Technical characteristics for an automatic identification system using time-division multiple access in the

VHF maritime mobile band. Recommendation ITU-R M.1371-4, April, 2010. http://www.itu.int/rec/R-REC-M.1371/en.

[12] Elin Dombestein, Amund Lorentz Gjersøe, Karl Thomas Hjelmervik, and Morten Kloster. *LYBIN 6.0 - user manual*. FFI (Norwegian Defence Research Establishment), Horten, Norway, 2011.

[13] Jens M. Hovem. *Marine Acoustics, The Physics of Sound in Underwater Environments*. Peninsula Publishing, Los Altos, California, USA, 2010.

[14] Leslie M. Gray and David S. Greeley. Source level model for propeller blade rate radiation for the world's merchant fleet. *J. Acoust. Soc. Am.*, 67(2):516–522, 1980.

[15] Stephen C. Wales and Richard M. Heitmeyer. An ensemble source spectra model for merchant ship-radiated noise. *The Journal of the Acoustical Society of America*, 111(3):1211–1231, 2002.

[16] Paul Scrimger and Richard M. Heitmeyer. Acoustic source-level measurements for a variety of merchant ships. *The Journal of the Acoustical Society of America*, 89(2):691–699, 1991.

[17] R. Otnes et al. *NGAS10 sea trials, Horten, Norway, June 2010.* FFI (Norwegian Defence Research Establishment), 2010. FFI-rapport 2010/01937.

[18] R. Otnes et al. *NGAS09 sea trials, Toronto, Italy, May 2009.* FFI (Norwegian Defence Research Establishment), 2009. FFI-rapport 2009/01637.

[19] Directional Passive Sonobuoy AN/SSQ-53D(3) Specification. Ultra Electronics, 2003.

[20] *Matlab toolbox for AIS messages, v 1.2.* Virtuelle Møre, Høgskolen i Ålesund, Online: http://vrmore.no/vm/om_prosjektet/publikasjoner/rapporter_og_programvare/matlab_toolbox_for_ais_messages, 2009.

[21] F. B. Jensen, W. A. Kuperman, M. B. Porter, and H. Schmidt. *Computational ocean acoustics*. Springer-Verlag, Springer New York Dordrecht Heidelberg London, 2011.

[22] Ellen Johanne Eidem. *Bottom types in LYBIN*. FFI (Norwegian Defence Research Establishment), 2011. FFI-notat 2011/00868.

[23] Lian S. Wang et al. Measurement of radiated ship noise. *ECUA 2012 11th European Conference on Underwater Acoustics*, 17(1):070091, 2013.

Appendix A

A current measurement standard

The ANSI standard ANSI/ASA S12.64-2009/Part 1 [7], describes the instrumentation, measurement requirements, procedures and the post processing on how to acquire the beam aspect underwater affected sound pressure level from a surface vessel. The following sections will give a summary of the standard.

A.1 Instrumentation

The standard has three different grades off accuracy for the measurement. The Grades are A, B and C, where A is the most accurate and complex method. The instrumentation parts of the system are the hydrophones, the signal acquisition and processing, and distance measurement. The grades have different requirements for these components, so that they can be chosen based on which grade of measurement is desirable.

The hydrophones should have an omni-directional sensitivity and the bandwidth and dynamic range specified by the respective grade. The number of hydrophones is also determined by the grade, and they are to be calibrated every 12 months.

The data acquisition system must be capable of accurately recording and processing the data from the hydrophones, and must fulfill Nyquist requirements. Grade A specifies that each of the three hydrophone channels must be recorded at the same time and be sample accurate. All grades specify that broadband processing is to be performed in 1/3 octave band, however the bandwidth is smaller for lower grades, starting at 10 - 50,000 Hz for Grade A. For Grade B the bands shall range from 20 to 25,000 Hz, and for Grade C, 50 to 10,000 Hz. Narrowband processing is

to be described in later parts of the standard, but is stated to be in appropriate bandwidths up to 5 kHz or higher as needed.

To determine the horizontal distance between the acoustic center of the ship and the place where the hydrophone is deployed a distance measurement system must be used, e.g. a GPS. For Grade A the distance must be measured continuously for the whole length, whereas for Grade B and C only the distance at the Closest Point of Approach (CPA) needs to be measured. The distance measurement system must have an accuracy of up to 2% of the distance at CPA for Grade A and B, and 5% for Grade C.

It is assumed that the ship is a point source with center that is halfway between the engine room and the propeller (Grade B and C). For Grade A the source center must be determined by the user, e.g. as the point where one has maximum output at the hydrophone along the track.

A.2 Measurement requirements and procedure

The test site for the measurement must have a minimum water depth of 300 m or three times the overall ship length for Grade A. For Grades B and C the water depth can be shallower. Other than that a test site location can be chosen freely, however vessel traffic, ambient noise, bottom type and such should be considered.

The wind speed during measurement should be less than 20 knots. Rough seas may impact source level measurement by increased noise and instability in the vessel. With that limitation, vessels with length greater than 100 m will have consistent source levels regarding noise caused by surface waves.

Three hydrophones in vertical alignment are required for Grades A and B. For Grade C only one hydrophone is needed. None shall be located on the seabed. They are to be placed at depths corresponding to angles 15°, 30° and 45° from the center of the vessel track at the surface, see Eq. (A.1), and with a horizontal distance of d_{CPA} which is the minimum distance at the Closest Point of Approach. For Grade C, the hydrophone is placed at a depth corresponding to a 20° ±5° angle. d_{CPA} should be the greater of 100 m or overall vessel length with ±10% tolerance. An illustration showing the hydrophone geometry for Grades A and B is seen in Figure A.1.

$$\text{Depth} = d_{\text{CPA}} \cdot \tan(\text{angle}). \tag{A.1}$$

The deployment method for the hydrophones can be chosen freely, but three methods are described. The hydrophones can be supported by a surface buoy with a suspension device, and either transmit remotely or by cable to a nearby support vessel. In the third method the hydrophones may be connected to a bottom anchor with signal lines going to shore, and a subsurface buoy.

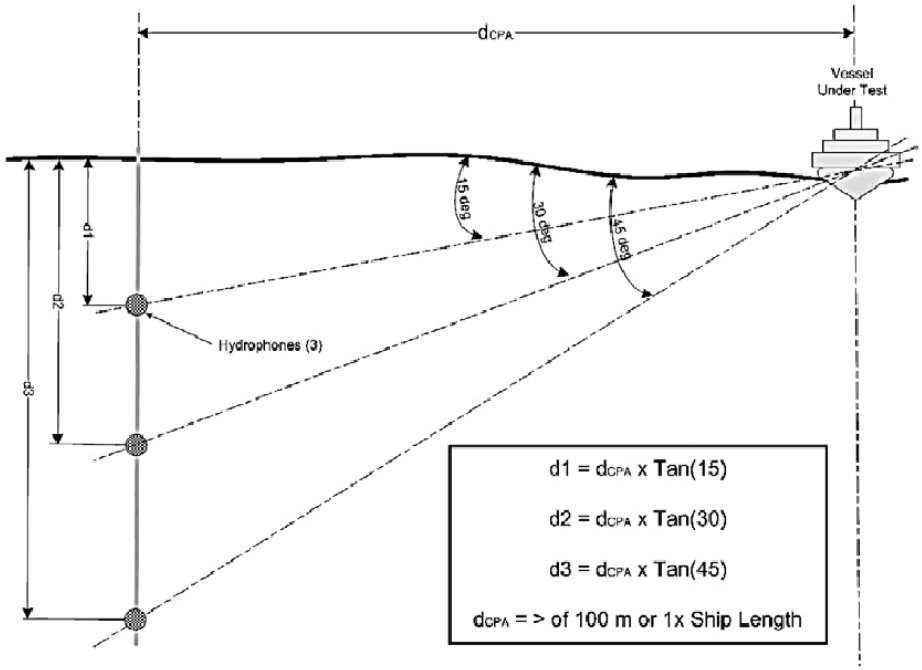

Figure A.1: An illustration showing the hydrophone geometry for Grades A and B [7].

The test course for the vessel is the same for all grades. It will proceed along a straight line past the CPA, starting at a position called COMEX (commence exercise), and finishing at FINEX (finish exercise). COMEX is two data window lengths (DWL) before CPA, and FINEX is the same distance after CPA. DWL will be defined in Section A.3. At the start of the measurement period background noise measurement shall be performed. The vessel is then moved 2 km away from the hydrophones and set to a quiet condition. After this the measurement can be started. When finishing one run the vessel will perform the Williamson curve to turn the ship and come back to repeat the measurement, until the desired number of runs have been reached. At COMEX the vessel shall keep all operating conditions constant until FINEX.

For Grade A three runs at each side of the ship for every vessel condition to be tested is necessary. For Grade B and C fewer runs are needed. Further details regarding communication are also described.

A.3 Post processing

After the measurements are completed, the signals must be processed to adjust for distance, sensitivity and noise if necessary. The result is source sound pressure levels (SPL) in dB re 1μPa normalized to 1 meter in one-third octave bands for varying frequency bands for the different grades. All adjustments are made to one-third octave data.

Except for the part that shows how to combine levels from the different hydrophones, the following is the same for all grades.

The part of the recorded signal that is to be used to analyse the SPL is defined by the data window length, which is depending on the data window angle. This angle is defined as $\pm 30°$ from the CPA. The standard then gives this formula for the DWL in meters:

$$\mathrm{DWL} = 2 \cdot d_{\mathrm{CPA}} \cdot \tan(\mathrm{angle}), \tag{A.2}$$

where angle=30° and 2·tan(30)≈1.15. This will give a DWL that is slightly longer than d_{CPA} or the vessel length. The corresponding data window period (DWP) is the time in seconds it takes the vessel to travel the DWL, and is given by

$$\mathrm{DWP} = \frac{\mathrm{DWL}}{v}, \tag{A.3}$$

where v is the vessel speed in m/s. For Grade A only, the DWL must be divided into no longer than 1 s long samples.

If the signal to background noise ratio is more than 3 dB and less than 10 dB in a one-third octave band, the signal in that band must be adjusted for the noise level. If it is more than 10 dB no adjustments are required, or if it is less than 3 dB, the measurement must be marked as such or disregarded. The background noise adjusted SPL is then found by subtracting the noise SPL from the signal including noise SPL like this,

$$L'_p = 10 \log_{10} \left(10^{(L_{p_{s+n}}/10)} - 10^{(L_{p_n}/10)} \right), \tag{A.4}$$

where $L_{p_{s+n}}$ is the signal with noise sound pressure level, L_{p_n} is the background noise sound pressure level, and L'_p is the noise adjusted SPL of the vessel.

Adjustments in the SPL should not be done to discrete frequency components, as it has shown to give undesired results.

In addition to noise adjustments, it must be adjusted for various sensitivities and gains in the system. If these adjustments can be summed to a general sensitivity factor A_{SEN}, then the sensitivity adjusted SPL can be written like this,

$$L''_p = L'_p + A_{SEN}. \tag{A.5}$$

After noise and sensitivity adjustments, the SPL must be adjusted for distance. The formula for the total distance (d_{Total}) to a hydrophone is

$$d_{Total} = \sqrt{d_{CPA}^2 + d_{Vert}^2(h)}. \tag{A.6}$$

d_{CPA} is the distance between the hydrophone and the vessel at CPA, and $d_{Vert}(h)$ is the depth of the hydrophone, where h can be the shallow (h1), middle (h2) or deep (h3) location of the hydrophone. As the standard uses a spherical spreading model, the source sound pressure level is

$$L_s(r, h) = L_p'' + 20\log_{10}(d_{Total}/d_{ref}), \tag{A.7}$$

where the reference distance d_{ref} is 1 m.

The next step is to combine the SPLs from the different hydrophones and runs. This is slightly different for the different grades, as they have different number of hydrophones and runs.

For Grade A and B, port and starboard runs shall be kept separate. For Grade A only three runs on each side is combined, and in those runs, the three hydrophone sets are combined. For Grade B, it is the same as for Grade A, except only two runs on each side is combined. For Grade C, all the runs are combined into one level for the single hydrophone.

The following formula is used to combine the data from the three hydrophones,

$$L_s(r) = 10\log_{10}\left((10^{(L_s(r,h1)/10)} + 10^{(L_s(r,h2)/10)} + 10^{(L_s(r,h3)/10)})/3\right) \tag{A.8}$$

The (k) different runs (r) are added together arithmetically to get the resulting signature source level:

$$L_s = \frac{\sum_{r=1}^{r=k} L_s(r)}{k}. \tag{A.9}$$

A.4 Uncertainty

The standard gives some uncertainty values for the resulting levels as guidance. For the instrumentation part, a combined uncertainty of 1.3 dB is stated as a typical value for the sound pressure level L_p. For the resulting source level L_s, the uncertainty for each hydrophone would normally be around 2 dB, but the average of the three hydrophones is less. The different grades have a stated total measurement uncertainty, which is how much the resulting level may deviate from the true level. For Grade A it is 1.5 dB, for Grade B it is 3.0 dB and for Grade C it is 4.0 dB. It also states the measurement repeatability, which is how much the resulting source level likely may differ from repeated measurements under the same

conditions. For Grade A it is ±1.0 dB, for Grade B it is ±2.0 dB and for Grade C it is ±3.0 dB.

For more details, see [7].

Appendix B

Analytical transmission loss

B.1 Surface reflection

An effect that contributes to the received sound level is the reflection from the surface, which comes in addition to the direct path sound [8] [10]. This effect is also called the Lloyd's mirror effect (LM), and an illustration of the set-up can be seen in Figure B.1. In the standard three hydrophones in vertical alignment are used, and the signals from them are averaged, which diminishes the effect from the surface reflection. As there is only one hydrophone in this model, this effect may be significant. The point source model presented next is coherent, such that the phase of the waves are taken into account.

B.2 Point source

Here a LM model with a point source will be described.

When one can assume a smooth surface, the reflection coefficient for the surface is -1,. This means a totally reflective, pressure release surface, with a 180° phase shift. One can then say there is a mirror source above the surface, and the total source is then effectively a dipole. When the distance is long, the difference in travelled distance between the direct path and the reflected path is small. The combination of the phase shift and the distance difference creates an interference pattern. The interference pattern is dependant on the depth of the source and the receiver, the horizontal distance between them and the frequency of the pressure wave.

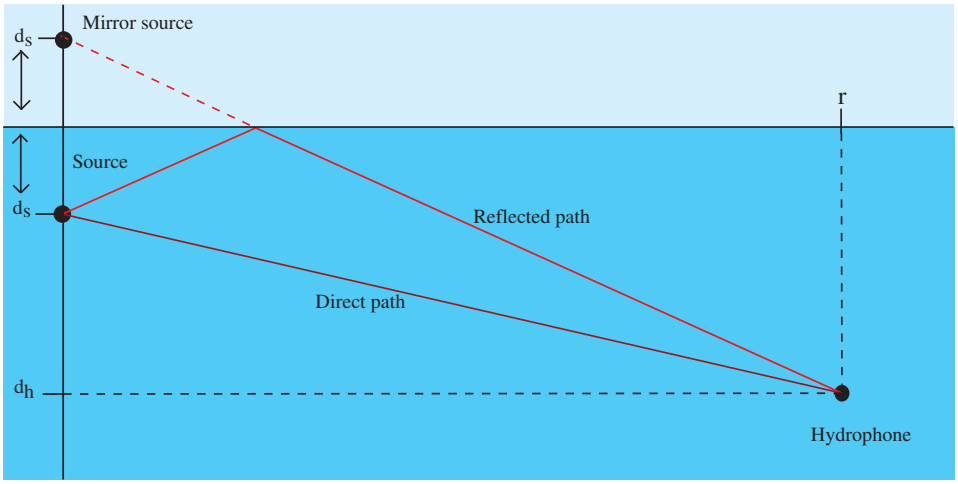

Figure B.1: An illustration showing surface reflection as an mirror source.

The two pressure waves can be described mathematically without time dependency as

$$p_d(r_d) = \exp(ikr_d), \tag{B.1}$$
$$p_r(r_r) = \exp(ikr_r), \tag{B.2}$$

where $p_d(r_d)$ is the direct pressure wave, $p_r(r_r)$ is the reflected pressure wave, r_d and r_r is the travelled distance for the two respective waves in meters, and k is the wave number

$$k = \frac{2\pi f}{c}. \tag{B.3}$$

Here f is the frequency of the wave and c is the speed of sound in water.

By looking at Figure B.1, one can see that the travelled distance for each of the waves can be written in terms of the depth of the source and receiver, d_s and d_h and the horizontal range r:

$$r_d = \sqrt{(d_h - d_s)^2 + r^2}, \tag{B.4}$$
$$r_r = \sqrt{(d_h + d_s)^2 + r^2}, \tag{B.5}$$

where d_h and d_s is the depth of the receiver and the source respectively in meters.

When a smooth pressure release surface is assumed, the reflection coefficient becomes $R_{coeff} = -1$. The resulting pressure wave at the point of the receiver is then

$$p = \left(\frac{\exp(ikr_d)}{r_d} - \frac{\exp(ikr_r)}{r_r} \right), \tag{B.6}$$

when considering spherical spreading.

According to Eq. (2.21) the analytical transmission loss for spherical spreading with surface reflection in decibel is then

$$TL = -10 \log_{10}(p^2). \tag{B.7}$$

Appendix C

Received level results

C.1 Thebe at NILUS-D

A spectrogram showing the RL of Thebe passing NILUS-D as frequency vs time can be seen in Figure C.1. From this one can see that the measurement is of low quality, that is, a low RL at CPA, and with possible interference from other unidentified ships.

The received level as pressure vs. frequency for the passing of Thebe at CPA recorded by NILUS-D can be seen in Figure C.2 for 1 Hz bands (left) and for 1/3 octave bands (right). The analysis time, or data window period, was 17 s. The broadband RL is 107.0 dB re $1\mu\text{Pa}^2$.

The background noise connected to Thebe and NILUS-D is chosen as a one minute period of low sound intensity about ten minutes after CPA. It is estimated as a received level. The received level for the background noise as pressure vs. frequency is plotted in Figure C.3 for 1 Hz bands (left) and for 1/3 octave bands (right). The broadband RL of the background noise is 94.8 dB re $1\mu\text{Pa}^2$.

The signal-with-noise to noise ratio (SNR) is the RL of Thebe minus the RL of the background noise. The SNR vs frequency for the passing of Thebe at CPA is plotted in Figure C.4 for 1 Hz bands (left) and for 1/3 octave bands (right).

For frequencies where the SNR is less than required, the RL is adjusted. This is the case here, as one can clearly see from Figure C.4. The adjusted RL vs frequency for Thebe at CPA is plotted in Figure C.5 for 1 Hz bands (left) and for 1/3 octave bands (right).

For the RL at CPA of Thebe at NILUS-D, the difference between the noise adjusted RL and the unadjusted RL vs frequency is plotted in Figure C.6 for 1 Hz bands (left) and for 1/3 octave bands (right). The differences are clearly visible in 1 Hz bands, as the SNR is low. The blue crosses indicate frequencies where the SNR

was lower than 3 dB. In 1/3 octave bands, the adjustment is significant for the 6 bands where the adjustment was necessary.

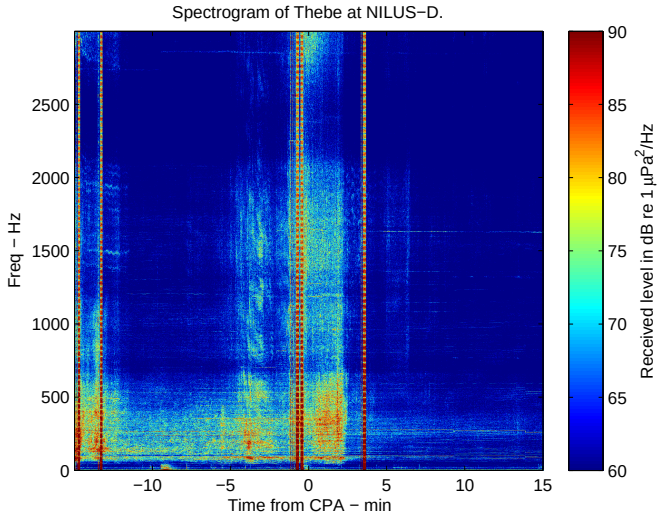

Figure C.1: Spectrogram of Thebe at NILUS-D.

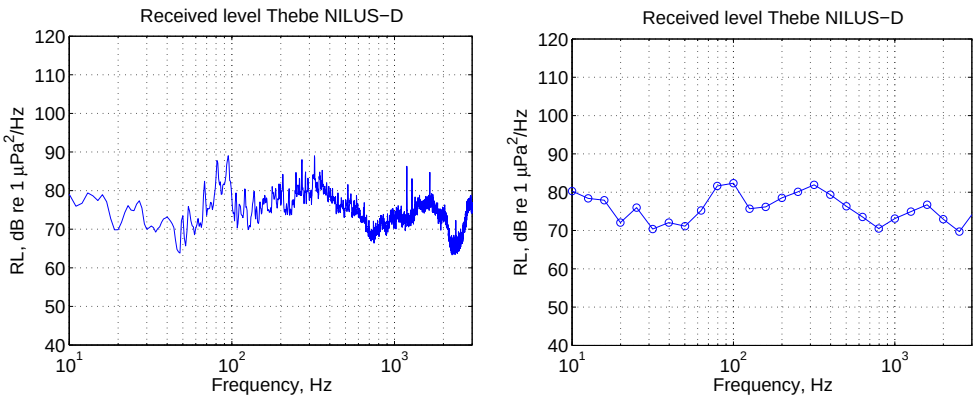

Figure C.2: Received level vs frequency of Thebe at NILUS-D in 1 Hz bands (left) and in 1/3 octave bands (right).

C.2 Autobank at NILUS-D

The CPA of Autobank passing NILUS-D coming from Drammen was 1564 m.

A spectrogram showing the RL of Autobank passing NILUS-D as frequency vs

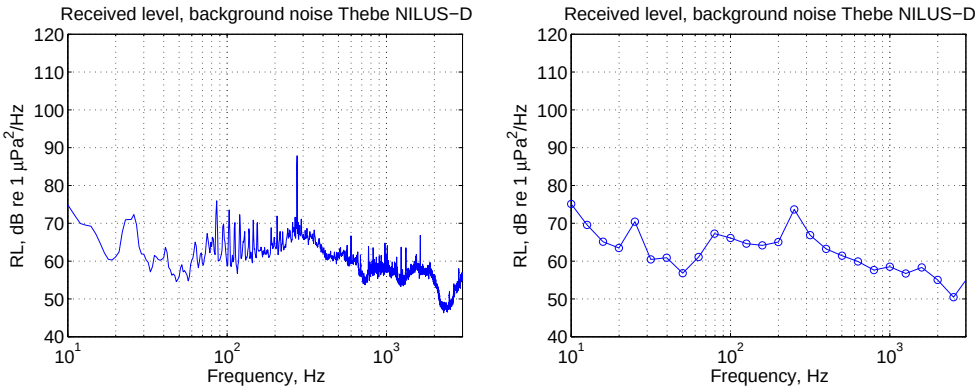

Figure C.3: Received level vs frequency for the background noise of Thebe at NILUS-D in 1 Hz bands (left) and in 1/3 octave bands (right).

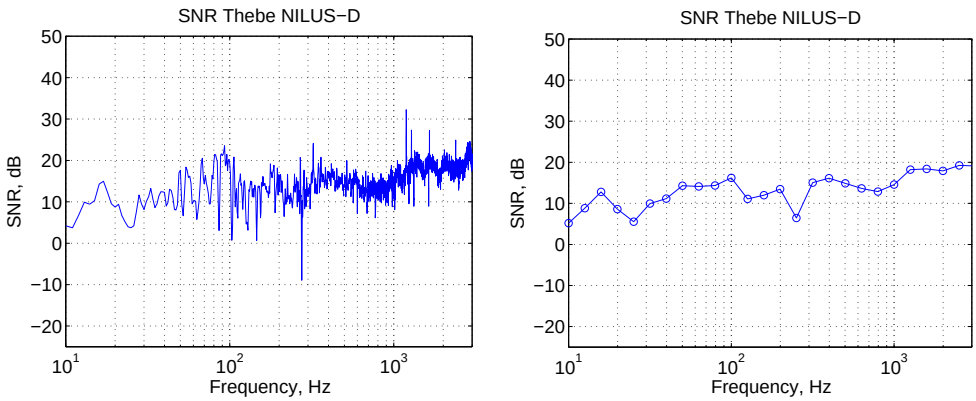

Figure C.4: The SNR vs frequency for Thebe at NILUS-D in 1 Hz bands (left) and in 1/3 octave bands (right).

time can be seen in Figure C.7. From the spectrogram one can see that the high intensity RL around CPA is slightly irregular and uncentered for a ship passing. It is not clear whether it is unidentified ships or the environment that is the cause of this.

The received level vs frequency at CPA is plotted in Figure C.8 for 1 Hz bands (left) and for 1/3 octave bands (right). The broadband RL is 121.3 dB re $1\mu\text{Pa}^2$.

The background noise connected to Autobank and NILUS-D is chosen as a 30 seconds period of low sound intensity about 18 minutes after CPA. The received level for the background noise as pressure vs. frequency is plotted in Figure C.9 for 1 Hz bands (left) and for 1/3 octave bands (right). The broadband RL of the background noise is 84.8 dB re $1\mu\text{Pa}^2$.

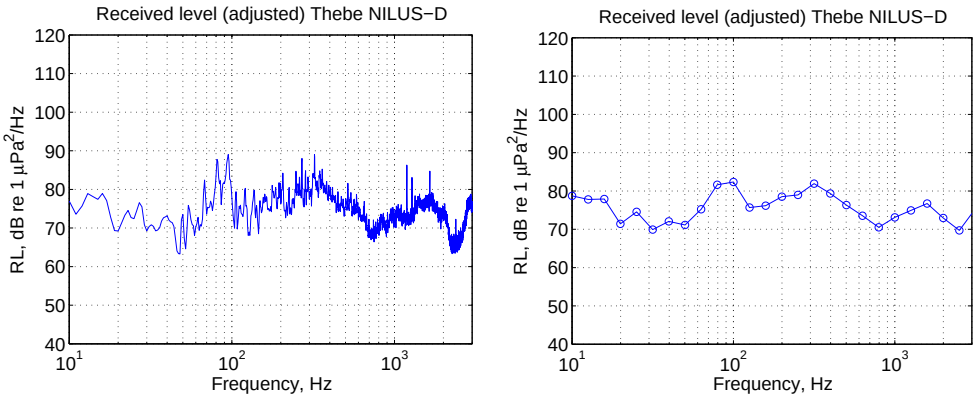

Figure C.5: Adjusted received level vs frequency of Thebe at NILUS-D in 1 Hz bands (left) and in 1/3 octave bands (right).

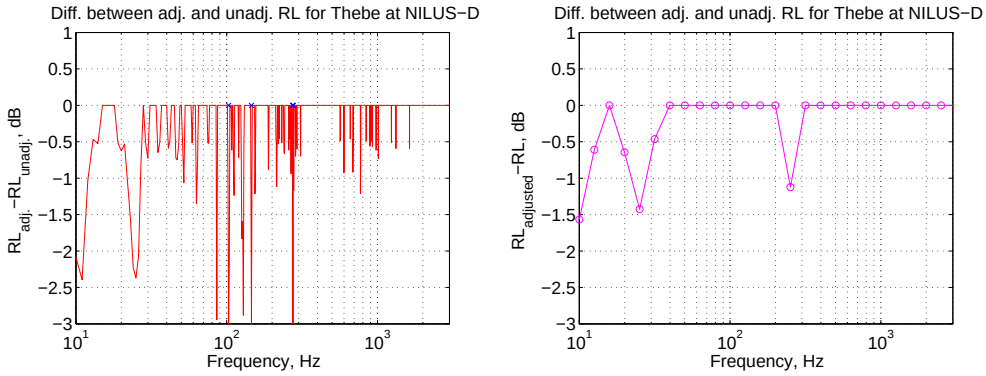

Figure C.6: Difference between noise adjusted RL and unadjusted RL vs frequency of Thebe at NILUS-D in 1 Hz bands (left) and in 1/3 octave bands (right).

The signal-with-noise to noise ratio (SNR) is the RL of Autobank minus the RL of the background noise. The SNR vs frequency for the passing of Autobank at CPA is plotted in Figure C.10 for 1 Hz bands (left) and for 1/3 octave bands (right).

The SNR is high, as the background noise was measured at a quiet period 18 minutes after the ship passing where there was little traffic. However there may be other sources interfering around CPA, but those are not included in the AIS information. As the SNR is within the requirements for the relevant frequencies, no adjustments are required.

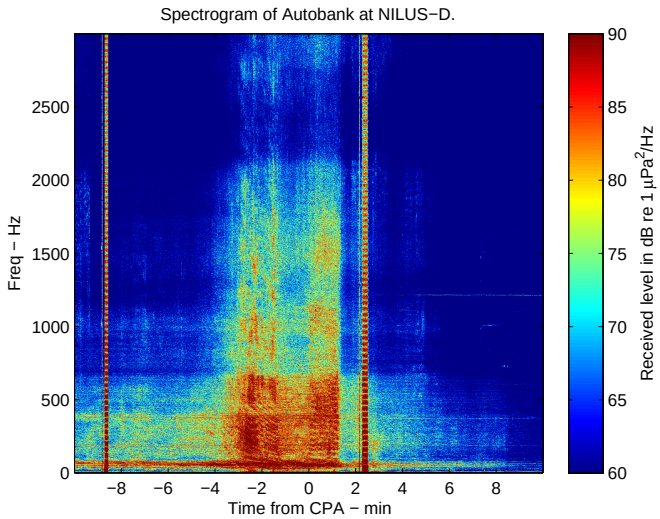

Figure C.7: Spectrogram of Autobank at NILUS-D.

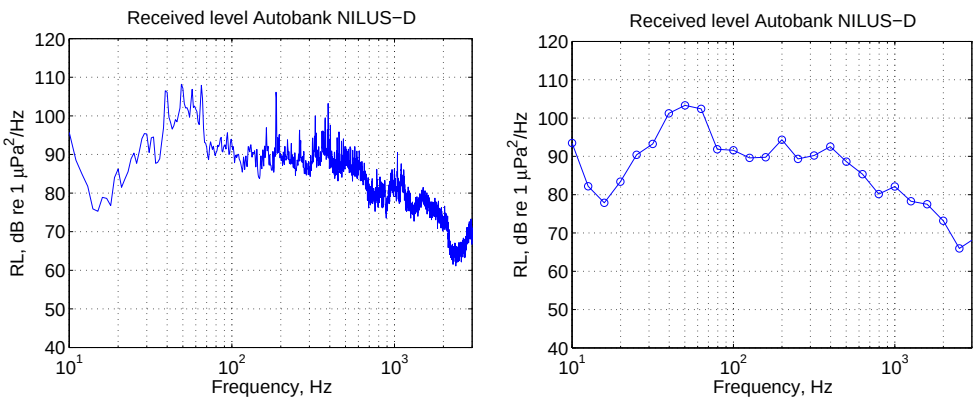

Figure C.8: Received level vs frequency of Autobank at NILUS-D in 1/3 octave bands.

C.3 Elektron II at NILUS-C

Because of the amplitude clipping of the recording near CPA, the measured RL and thus SL is taken as the average of a measurement before and after the visible clipping, each with a measurement time according to the DWP (17 s). The CPA of Elektron at NILUS-C was 540 m. The measurement of the ship before CPA was 2:30 minutes prior the CPA, and at a horizontal distance of 1015 m from the node. The measurement after CPA was 1:46 minutes after CPA, at a horizontal distance of 772 m from the node. This yields an aspect angle of 32.2 degrees (re bow) before

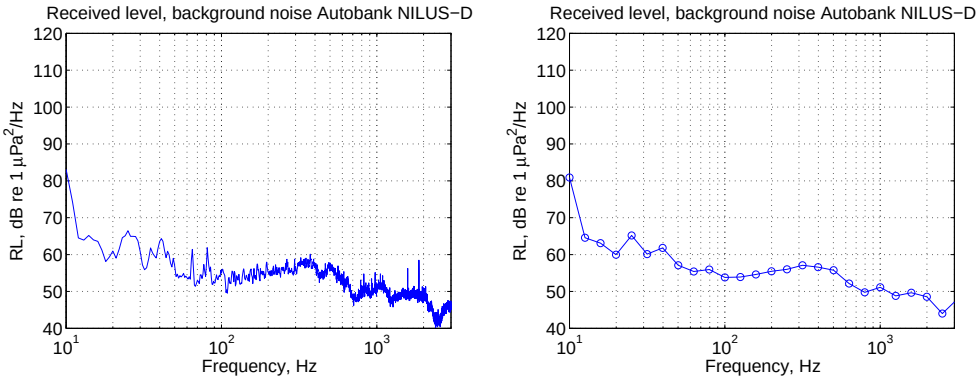

Figure C.9: Received level vs frequency for the background noise of Autobank at NILUS-D in 1 Hz bands (left) and in 1/3 octave bands (right).

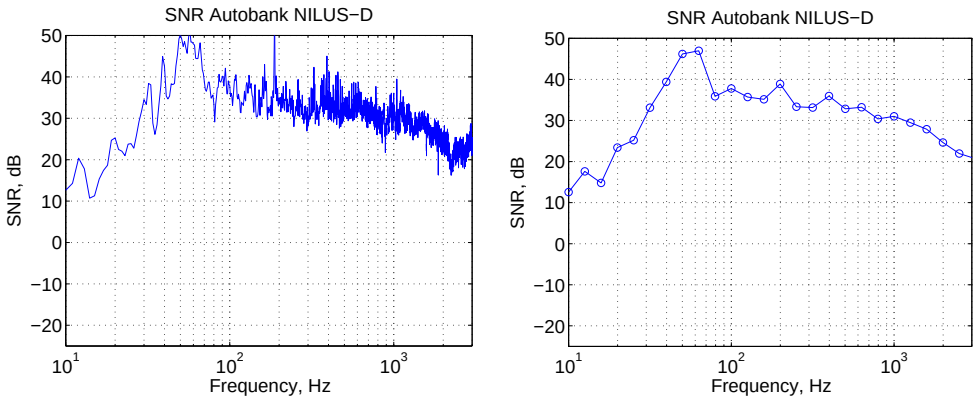

Figure C.10: The SNR vs frequency for Autobank at NILUS-D in 1 Hz bands (left) and in 1/3 octave bands (right).

CPA, and 135.5 degrees (re bow) after CPA.

A spectrogram showing the RL of Elektron passing NILUS-C as frequency vs time can be seen in Figure C.11. From the spectrogram one can see that the RL is higher before CPA than after CPA.

The received level vs frequency before and after CPA is plotted in Figure C.12 for 1 Hz bands (left) and for 1/3 octave bands (right). The broadband RL before CPA was 127.1 dB re 1μPa^2, and 124.5 dB re 1μPa^2 after CPA.

The averaged RL vs frequency for Elektron is plotted in Figure C.13 for 1 Hz bands (left) and for 1/3 octave bands (right). The average broadband RL is 125.8 dB re 1μPa^2.

The background noise connected to Elektron and NILUS-C is chosen as a 30 seconds

period of low sound intensity about 1 hour and 33 minutes after CPA. The received level for the background noise as pressure vs. frequency is plotted in Figure C.14 for 1 Hz bands (left) and for 1/3 octave bands (right). The broadband RL of the background noise is 105.2 dB re $1\mu\text{Pa}^2$.

The SNR vs frequency (the RL is the average of the RL before and after CPA) of Elektron is plotted in Figure C.15 for 1 Hz bands (left) and for 1/3 octave bands (right). The SNR is low in this case as there was much traffic in the time period surrounding the ship passing, and thus the background noise was high.

The average noise adjusted RL vs frequency for Elektron is plotted in Figure C.16 for 1 Hz bands (left) and for 1/3 octave bands (right). The average noise adjusted broadband RL is 125.1 dB re $1\mu\text{Pa}^2$.

For the RL at CPA of Elektron at NILUS-C, the difference between the noise adjusted RL and the unadjusted RL vs frequency is plotted in Figure C.17 for 1 Hz bands (left) and for 1/3 octave bands (right). The differences are clearly visible in 1 Hz bands and in 1/3 octave bands, as the SNR is low. The blue crosses indicate frequencies where the SNR was lower than 3 dB.

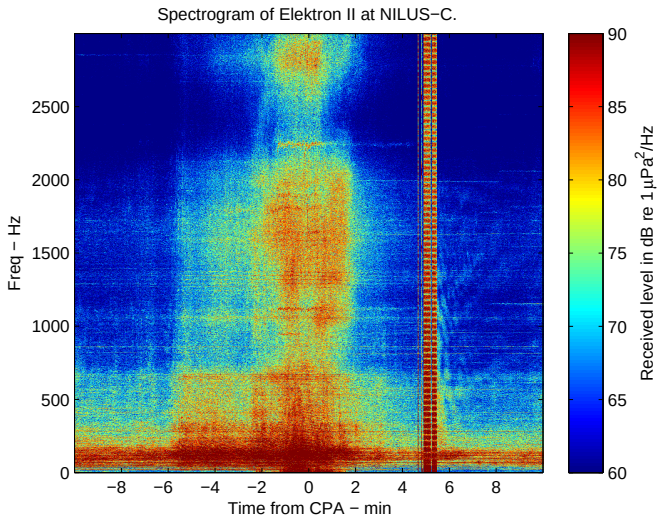

Figure C.11: Spectrogram of Elektron at NILUS-C.

C.4 Wilson Husum at NILUS-C

Because of the amplitude clipping of the recording near CPA, the measured RL and thus SL is taken as the average of a measurement before and after the visible clipping, each with a measurement time according to the DWP (17 s). The horizontal distance between Wilson Husum and NILUS-C at CPA was 84 m. The

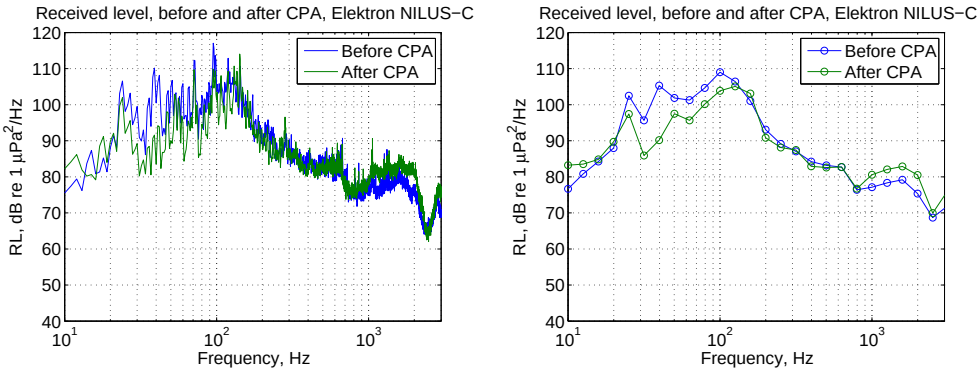

Figure C.12: Received level vs frequency of Elektron before and after CPA at NILUS-C in 1 Hz bands (left) and in 1/3 octave bands (right).

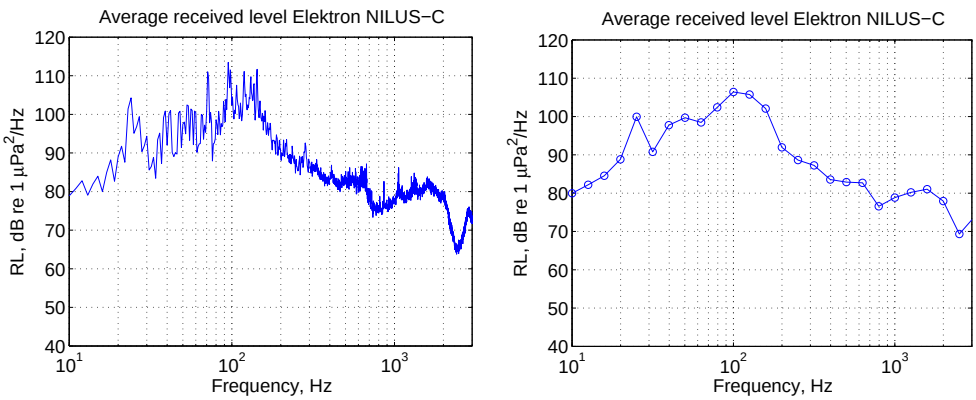

Figure C.13: Averaged received level vs frequency of Elektron at NILUS-C in 1/3 octave bands.

measurement of the ship before CPA was 2:05 minutes prior the CPA, and at a horizontal distance of 783 m from the node. The measurement after CPA was 1:18 minutes after CPA, at a horizontal distance of 491 m from the node. This yields an aspect angle of 6.2 degrees (re bow) before CPA, and 170.1 degrees (re bow) after CPA.

A spectrogram showing the RL of Wilson Husum passing NILUS-C towards Drammen as frequency vs time can be seen in Figure C.18. From the spectrogram one can see that the RL is high at CPA, but also 4 minutes before CPA. The spectral characteristics visible from the spectrogram indicate that the noise at CPA and 4 minutes before comes from the same source. So it is probably the environment that is causing the change in RL during the ship passing.

The received level vs frequency before and after CPA is plotted in Figure C.19 for

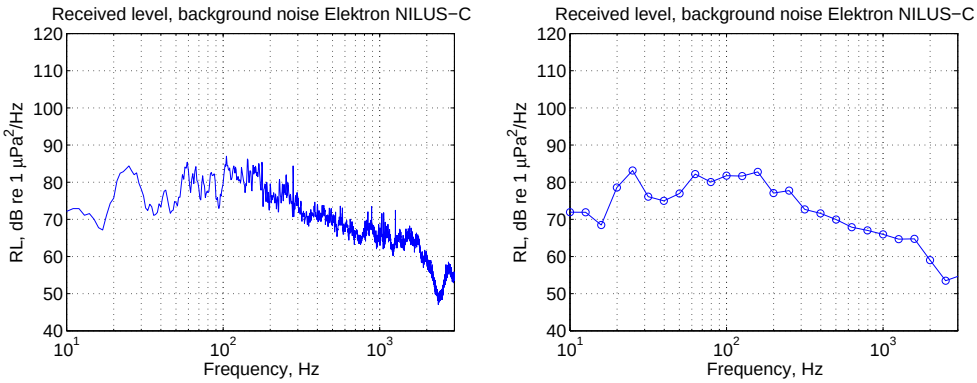

Figure C.14: Received level vs frequency for the background noise of Elektron at NILUS-C in 1 Hz bands (left) and in 1/3 octave bands (right).

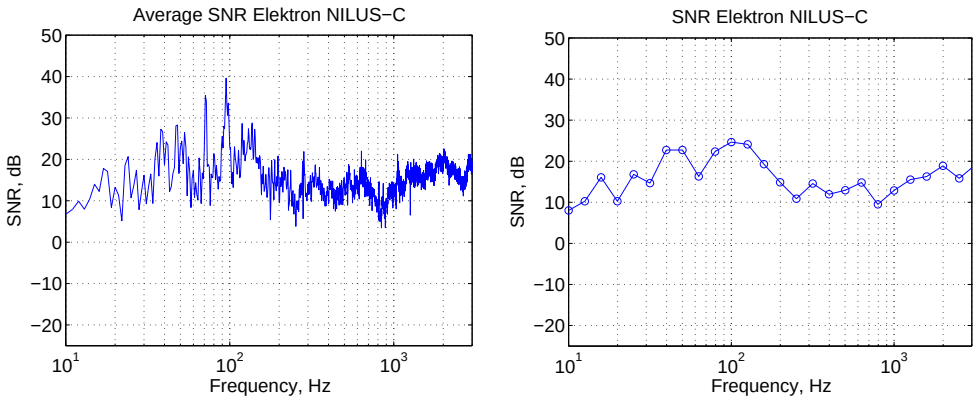

Figure C.15: The SNR vs frequency for Elektron at NILUS-C in 1 Hz bands (left) and in 1/3 octave bands (right).

1 Hz bands (left) and for 1/3 octave bands (right). The broadband RL before CPA was 126.1 dB re 1μPa^2, and 122.5 dB re 1μPa^2 after CPA.

The averaged RL vs frequency for Wilson Husum is plotted in Figure C.20 for 1 Hz bands (left) and for 1/3 octave bands (right). The average broadband RL is 123.8 dB re 1μPa^2.

The background noise connected to Wilson Husum and NILUS-C is chosen as a 30 seconds period of low sound intensity about 23 minutes before CPA. The received level for the background noise as pressure vs. frequency is plotted in Figure C.21 for 1 Hz bands (left) and for 1/3 octave bands (right). The broadband RL of the background noise is 101.6 dB re 1μPa^2.

The SNR vs frequency (the RL is the average of the RL before and after CPA) of

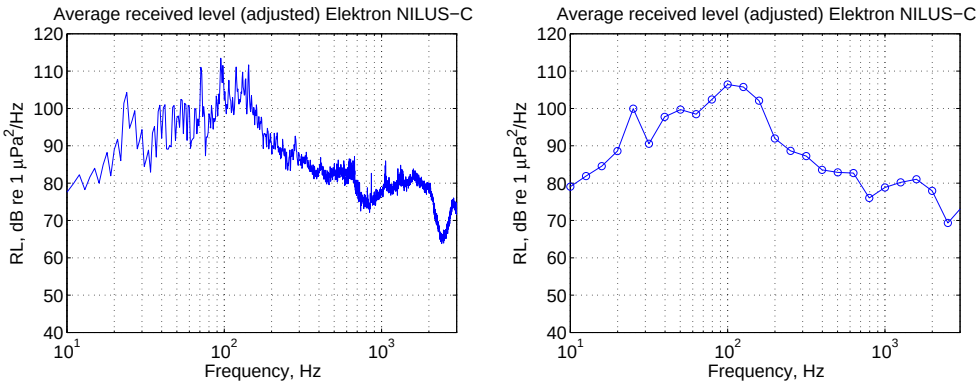

Figure C.16: Average adjusted received level vs frequency of Elektron at NILUS-C in 1 Hz bands (left) and in 1/3 octave bands (right).

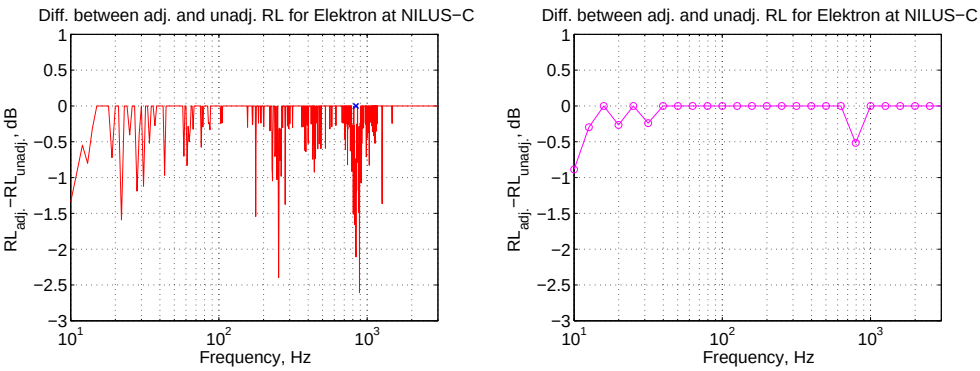

Figure C.17: Difference between noise adjusted RL and unadjusted RL vs frequency of Elektron at NILUS-C in 1 Hz bands (right) and in 1/3 octave bands (left).

Wilson Husum is plotted in Figure C.22 for 1 Hz bands (left) and for 1/3 octave bands (right). The SNR is not very high, but it is within the requirements so no adjustments to the RL are made.

C.5 Wilson Husum at NILUS-D

A spectrogram showing the RL of Wilson Husum passing NILUS-D as frequency vs time can be seen in Figure C.23. From this one can see that the measurement is of low quality, that is, a low RL at CPA, and with possible interference from other ships.

The received level as pressure vs. frequency for the passing of Wilson Husum at

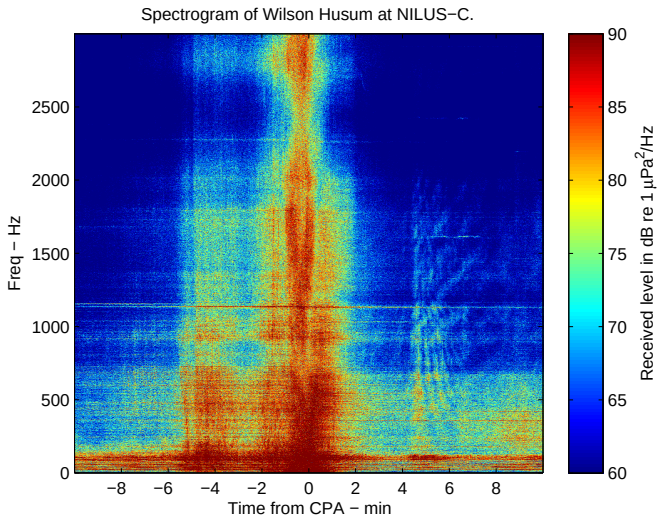

Figure C.18: Spectrogram of Wilson Husum at NILUS-C.

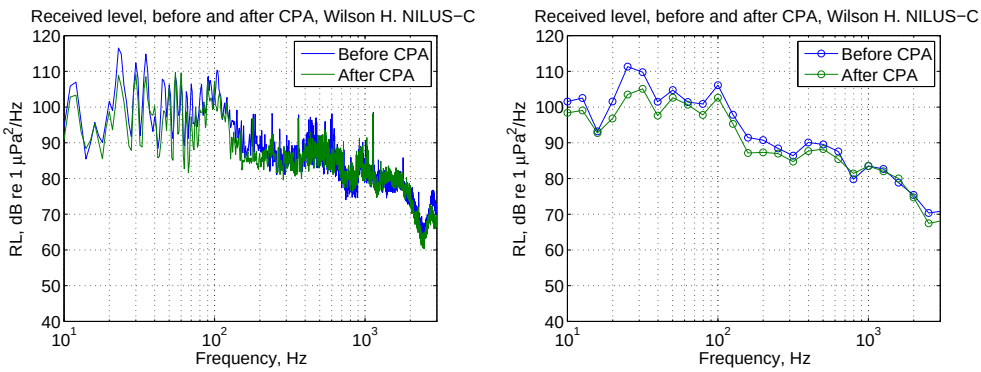

Figure C.19: Received level vs frequency of Wilson Husum before and after CPA at NILUS-C in 1 Hz bands (left) and in 1/3 octave bands (right).

CPA recorded by NILUS-D can be seen in Figure C.24 for 1 Hz bands (left) and for 1/3 octave bands (right). The analysis time, or data window period, was 16 s. The broadband RL is 113.4 dB re $1\mu\text{Pa}^2$.

The background noise connected to Wilson Husum and NILUS-D is chosen as a 30 second period of low sound intensity ten minutes before CPA. The received level for the background noise as pressure vs. frequency is plotted in Figure C.25 for 1 Hz bands (left) and for 1/3 octave bands (right). The broadband RL of the background noise is 96.7 dB re $1\mu\text{Pa}^2$.

The SNR vs frequency for the passing of Wilson Husum at CPA is plotted in Figure

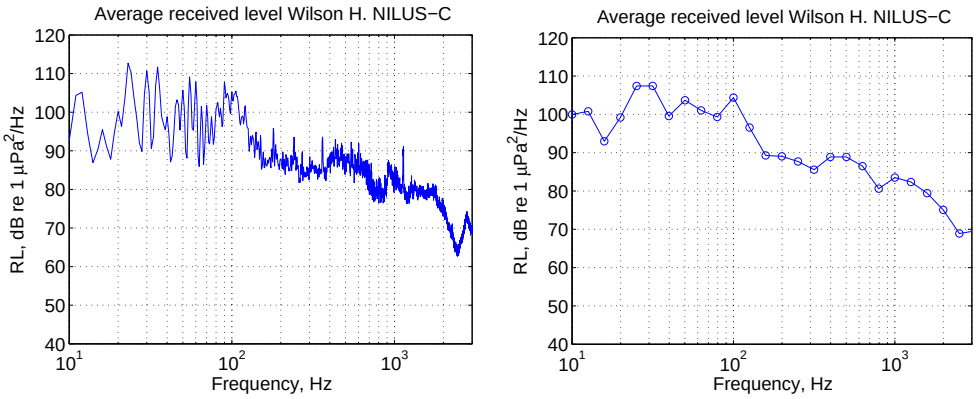

Figure C.20: Averaged received level vs frequency of Wilson Husum at NILUS-C in 1/3 octave bands.

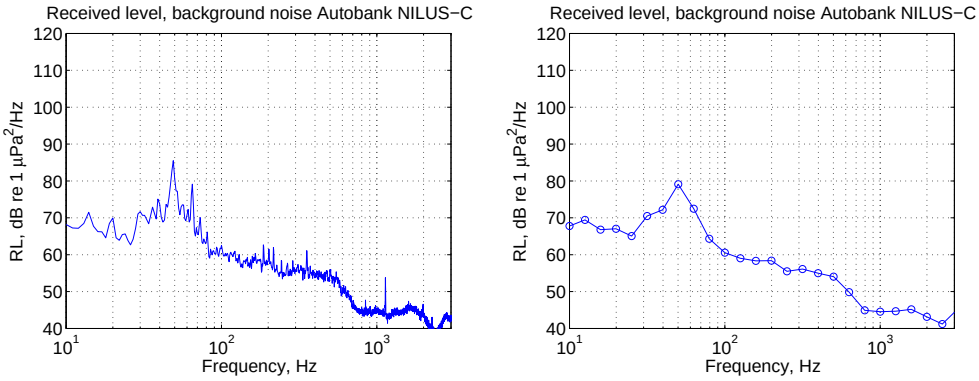

Figure C.21: Received level vs frequency for the background noise of Autobank at NILUS-C in 1 Hz bands (left) and in 1/3 octave bands (right).

C.26 for 1 Hz bands (left) and for 1/3 octave bands (right). As the SNR is below the requirements for some frequencies, adjustments are made. The adjusted RL vs frequency for Wilson Husum at CPA is plotted in Figure C.27 for 1 Hz bands (left) and for 1/3 octave bands (right).

For the RL at CPA of Wilson Husum at NILUS-D, the difference between the noise adjusted RL and the unadjusted RL vs frequency is plotted in Figure C.28 for 1 Hz bands (left) and for 1/3 octave bands (right). The differences are clearly visible in 1 Hz bands, as the SNR is low. The blue crosses indicate frequencies where the SNR was lower than 3 dB. In 1/3 octave bands, the adjustment is significant for the two bands where the adjustment was necessary.

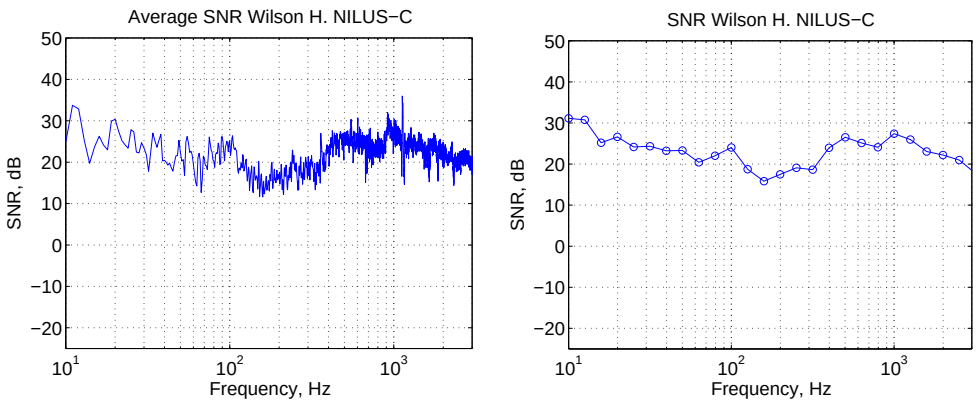

Figure C.22: The SNR vs frequency for Wilson Husum at NILUS-C in 1 Hz bands (left) and in 1/3 octave bands (right).

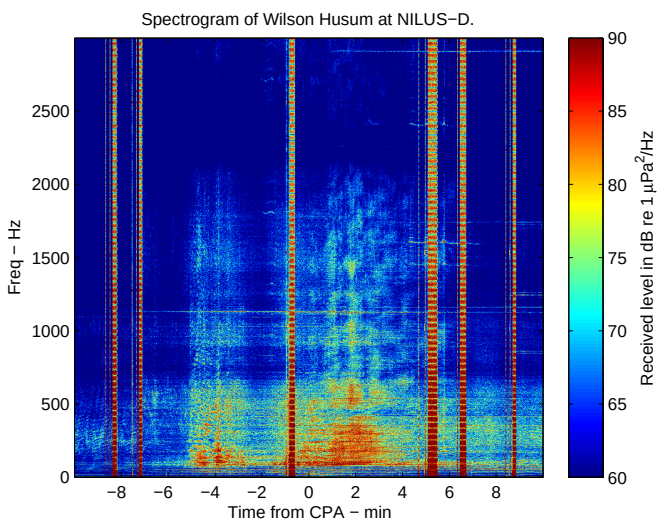

Figure C.23: Spectrogram of Wilson Husum at NILUS-D.

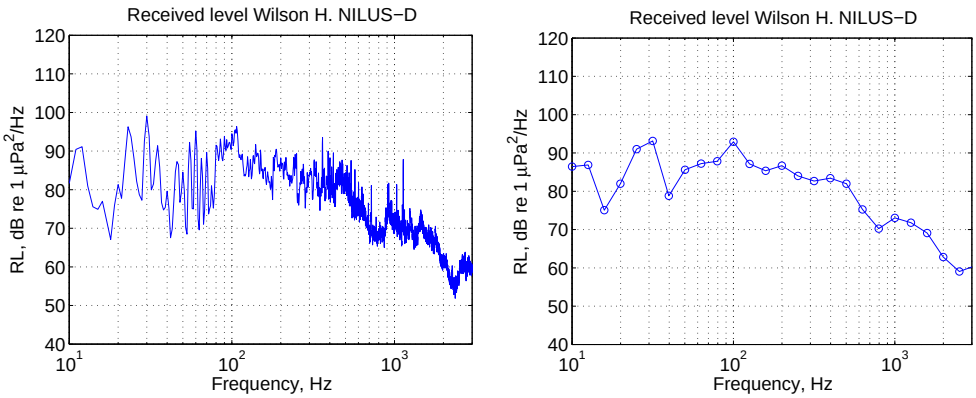

Figure C.24: Received level vs frequency of Wilson Husum at NILUS-D in 1/3 octave bands.

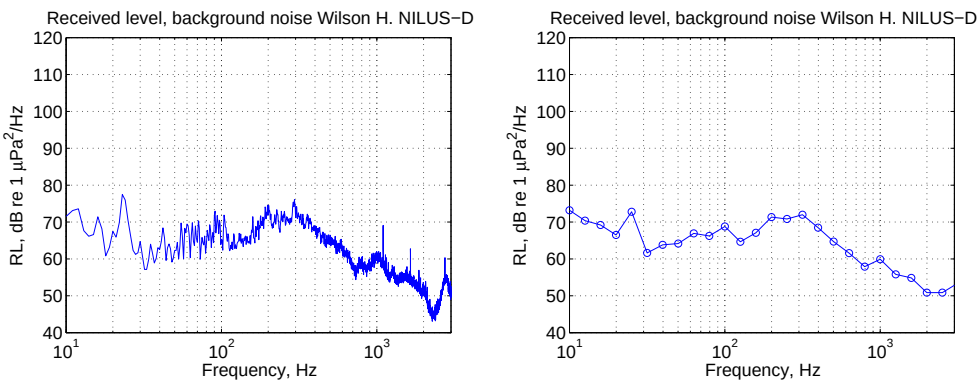

Figure C.25: Received level vs frequency for the background noise of Wilson Husum at NILUS-D in 1 Hz bands (left) and in 1/3 octave bands (right).

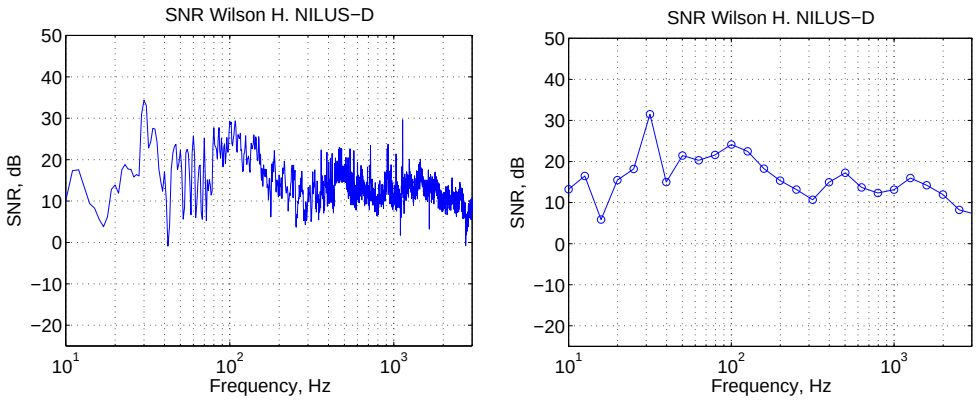

Figure C.26: The SNR vs frequency for Wilson Husum at NILUS-D in 1 Hz bands (left) and in 1/3 octave bands (right).

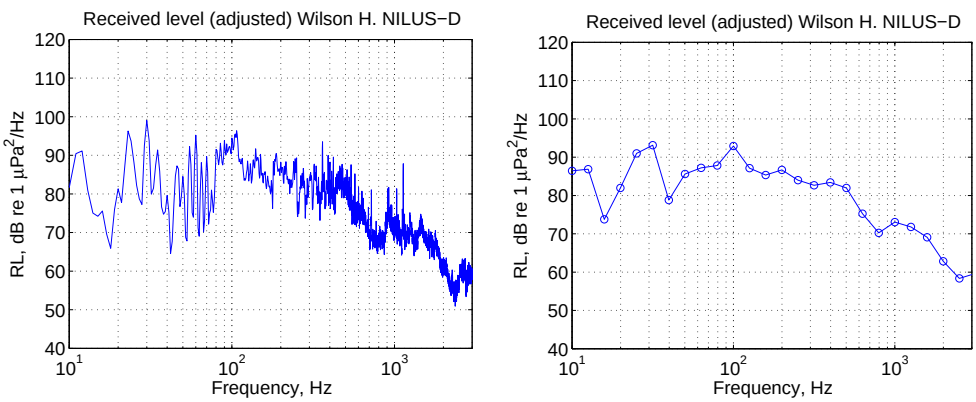

Figure C.27: Adjusted received level vs frequency of Wilson Husum at NILUS-D in 1 Hz bands (left) and in 1/3 octave bands (right).

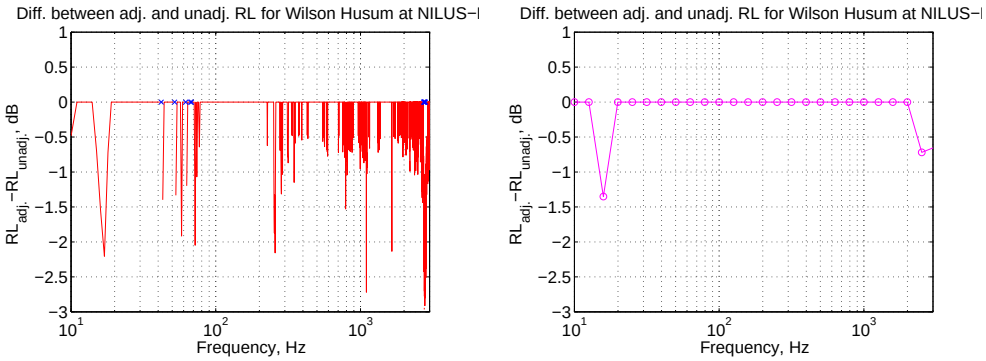

Figure C.28: Difference between noise adjusted RL and unadjusted RL vs frequency of Wilson Husum at NILUS-D in 1 Hz bands (left) and in 1/3 octave bands (right).